University of Alberta

PAPR Reduction Techniques in Wireless LAN Transceivers

by

Ali Alavi

A thesis submitted to the Faculty of Graduate Studies and Research in partial fulfillment of the requirements for the degree of **Master of Science**.

Department of Electrical and Computer Engineering

Edmonton, Alberta
Spring 2005

0-494-08019-1

Library and Archives Canada

Published Heritage Branch

395 Wellington Street
Ottawa ON K1A 0N4
Canada

Bibliothèque et Archives Canada

Direction du Patrimoine de l'édition

395, rue Wellington
Ottawa ON K1A 0N4
Canada

Your file *Votre référence*
ISBN:
Our file *Notre reference*
ISBN:

NOTICE:
The author has granted a non-exclusive license allowing Library and Archives Canada to reproduce, publish, archive, preserve, conserve, communicate to the public by telecommunication or on the Internet, loan, distribute and sell theses worldwide, for commercial or non-commercial purposes, in microform, paper, electronic and/or any other formats.

The author retains copyright ownership and moral rights in this thesis. Neither the thesis nor substantial extracts from it may be printed or otherwise reproduced without the author's permission.

AVIS:
L'auteur a accordé une licence non exclusive permettant à la Bibliothèque et Archives Canada de reproduire, publier, archiver, sauvegarder, conserver, transmettre au public par télécommunication ou par l'Internet, prêter, distribuer et vendre des thèses partout dans le monde, à des fins commerciales ou autres, sur support microforme, papier, électronique et/ou autres formats.

L'auteur conserve la propriété du droit d'auteur et des droits moraux qui protège cette thèse. Ni la thèse ni des extraits substantiels de celle-ci ne doivent être imprimés ou autrement reproduits sans son autorisation.

In compliance with the Canadian Privacy Act some supporting forms may have been removed from this thesis.

While these forms may be included in the document page count, their removal does not represent any loss of content from the thesis.

Conformément à la loi canadienne sur la protection de la vie privée, quelques formulaires secondaires ont été enlevés de cette thèse.

Bien que ces formulaires aient inclus dans la pagination, il n'y aura aucun contenu manquant.

Canada

To my parents Elaheh, Hossin

and my brother, Amir

Abstract

Orthogonal frequency division multiplexing (OFDM) overcomes the problem of multi-path fading in wireless communications. However, the potentially high peak-to-average-power ratio (PAPR) of OFDM is a drawback of this modulation. The use of Golay sequences can limit the PAPR in OFDM signals. In the first part of the thesis, we consider efficient maximum-likelihood decoding (MLD) of the Golay sequences by using the principle of sphere decoding. Our algorithms result in maximum likelihood BER performance and require substantially fewer computational operations than other known MLD algorithms. We also study the design of an efficient optimizer for the partial-transmit-sequence and we introduce a low-complexity optimization algorithm that offers optimum PAPR reduction performance. Lastly, we investigate the effect of channel coding on a class of transceivers which employ standard array of linear block codes (STA), to reduce the sensitivity of the transceivers to channel distortion.

Acknowledgements

I would like to express my sincere gratitude to Dr. Chintha Tellambura for his invaluable time, endless support and advice. I believe that working under his supervision has been a great honor and an unforgettable memory for me. I am grateful to Dr. Ivan Fair for his kind suggestions and generous supports. I would like to thank Dr. Marquez for his patience and invaluable advice during Summer 2003. I would also like to thank Dr. Witold Krzymien for his kind support.

I wish to record my gratitude to my beloved parents Elaheh and Hossin and my beloved brother Amir for their patience and continuous support. Special thanks goes to the colleagues of my research group for their help and co-operation. Finally, I would like to thank Department of Electrical Engineering at the University of Alberta for the invaluable support.

Contents

1 Introduction 1
- 1.1 Thesis Outline and Contributions . . . 2

2 Literature Review 4
- 2.1 Wireless LAN Standards . . . 4
  - 2.1.1 802.11a: High-Speed, High Capacity in the 5 GHz Band 5
  - 2.1.2 802.11g: High-Speed in the 2.4 GHz Band . . . 6
- 2.2 Orthogonal Frequency Division Multiplexing . . . 7
- 2.3 OFDM Over Wireless Channels . . . 9
  - 2.3.1 Channel model for frequency selective fading channels . . 10
- 2.4 Peak-To-Average-Power ratio . . . 11
  - 2.4.1 Definition of PAPR . . . 12
  - 2.4.2 PAPR Approximation Using Oversampling . . . 13
  - 2.4.3 Statistics of PAPR . . . 15
- 2.5 High Power Amplifier and Nonlinearity . . . 17
  - 2.5.1 Nonlinearity Models . . . 18
  - 2.5.2 Theoretical Performance Analysis Of OFDM Systems In The Existence Of Nonlinearity . . . 23
- 2.6 PAPR Reduction Techniques . . . 24
  - 2.6.1 Signal Distortion Techniques . . . 25
  - 2.6.2 Probabilistic Multiple Signalling . . . 27
  - 2.6.3 Block Coding . . . 32
- 2.7 Conclusion . . . 34

3 Efficient Decoding of Golay Sequences 36
- 3.1 Background . . . 36
- 3.2 Existing Decoding Techniques . . . 38
- 3.3 Reduced Complexity ML Decoding . . . 40
  - 3.3.1 Proposed Decoding Algorithm (Algorithm 1) . . . 42
  - 3.3.2 Initial Choice of The Radius of Sphere (μ) . . . 46
  - 3.3.3 Using Improved Lower Bounds in Algorithm 1 . . . 47
- 3.4 Numerical results . . . 48
  - 3.4.1 Performance of The Proposed Decoding Algorithms in AWGN and Fading Channels . . . 48
- 3.5 Conclusion . . . 56

4 Extension of The Proposed Algorithm and Complexity Analysis **57**
4.1 Decoding Low PAPR QAM Sequences Based on Golay Sequences 57
4.2 Performance of 16-QAM OFDM In Nonlinear Channels 59
4.3 Application of The Proposed Decoder in Differential M-ary DPSK-OFDM 59
4.3.1 Differential Detection 62
4.3.2 Performance Evaluation of the New MDPSK Receiver . . 64
4.4 Complexity Analysis of The Proposed Decoding Technique . . . 66
4.5 Conclusion 68

5 Design of Low Complexity Optimizer for the Partial Transmit Sequence Technique **69**
5.1 Overview of PTS 69
5.1.1 Existing Optimizers 72
5.2 New FPSD-based PTS Optimizer 73
5.2.1 Simulation Results 76
5.3 Conclusion 78

6 PAPR Reduction using Standard Array of Linear Block Codes **79**
6.1 STA-Based OFDM Transmitter and Receiver Architecture . . . 80
6.2 Performance Evaluation of STA-Based OFDM Transceivers in Ideal Communications Channel 81
6.3 STA-Based OFDM Transceivers in Non-Ideal Channels 85
6.4 Impact of Channel Encoding on STA Transceivers 86
6.4.1 STA-Based Transceiver Using Turbo-Codes 86
6.4.2 STA-Based Transceiver Using Convolutional Codes . . . 88
6.5 Conclusion 91

7 Conclusion **94**

Bibliography **97**

List of Figures

2.1 Typical channel profile for indoor office area with moderate delay spread 11
2.2 Amplitude (AM/AM) characteristic of a soft limiter 19
2.3 Amplitude (AM/AM) and phase (AM/PM) characteristics of TWTA 21
2.4 Amplitude (AM/AM) characteristic of SSPA 22
2.5 Block diagram of an OFDM transmitter with selected mapping 28
2.6 Block diagram of an OFDM transmitter using partial transmit sequence (PTS) 30
2.7 Block diagram of the interleaved OFDM transmitter 31

3.1 (a) Illustration of MLD for the RM(8, 4) BPSK code and SNR_b = 7 dB. (b) Illustration of Algorithm 1 for the RM(8, 4) BPSK code and $SNR_b = 7$ dB. 45
3.2 BER comparison for MLD, Algorithm 1, OSD and majority logic decoding for RM(16,5) in an AWGN channel using 8-PSK modulation. Note that the MLD and Algorithm 1 curves coincide exactly. 49
3.3 BER comparison for MLD, Algorithm 1, OSD and majority logic decoding for RM(32,6) in an AWGN channel using QPSK modulation. Note that the MLD and Algorithm 1 curves coincide exactly. 50
3.4 BER comparison for MLD, Algorithm 1, OSD and majority logic decoding for RM(16,5) in a fading channel using 8-PSK modulation. Note that the MLD and Algorithm 1 curves coincide exactly. 51
3.5 BER comparison for MLD, Algorithm 1, OSD and majority logic decoding for RM(32,6) in a fading channel using QPSK modulation. Note that the MLD and Algorithm 1 curves coincide exactly. 52
3.6 Number of codewords in the constructed spheres for first order Reed-Muller codes with 8-PSK and 32-PSK modulation. 53
3.7 Comparison of the number of required complex multiplications in MLD, Algorithm 1 and OSD. 54
3.8 Comparison of the number of required complex multiplications in Algorithm 1 and Algorithm 2. 55

4.1 BER performance of RM(8, 4) coded and uncoded QAM-OFDM with nonlinear amplifiers. 60
4.2 BER comparison for ML, Proposed Algorithm and OSD for RM(16,5) in a fading channel with 8-DPSK 63
4.3 BER comparison for ML, Proposed Algorithm and OSD for RM(16,5) in a fading channel with QDPSK 64
4.4 Decoding time comparison for ML, Proposed Algorithm and OSD for RM(16,5). 65

5.1 CCDF of the PAPR for exhaustive search, proposed optimizer and flipping algorithm 76
5.2 Comparison of the optimizing time required in exhaustive search, proposed optimizer and flipping algorithm 77

6.1 Block diagram of the STA transmitter 80
6.2 Block diagram of the STA receiver 82
6.3 CCDF of PAPR for STA transmitter with different number of branches 83
6.4 PSD of the OFDM signals with and without STA and with linear and nonlinear HPA 84
6.5 Bit Error Rate of an STA-Based Transceiver over an AWGN channel with a turbo code as the outer code 87
6.6 CCDF of PAPR of OFDM signals using convolutional coding and using uncoded BPSK vectors of length 32, 64 and 128 . . . 89
6.7 BER performance of STA transceiver without a nonlinear HPA and with nonlinear HPAs with convolutional code as outer code 90
6.8 PSD of the OFDM signals with and without STA and with linear and nonlinear HPA with QPSK and $n = 128$. 91
6.9 BER performance of STA transceiver without and with nonlinear HPA with different levels of nonlinearity in Rayleigh fading channel. QPSK modulation is used for data vectors of length $n = 128$. 92

List of Symbols

Acronyms	Definition
BER	bit error rate
CCDF	complementary cumulative distribution function
CCK	complementary-code-keying
CF	crest factor
CSI	channel state information
DSP	digital signal processing
DSSS	direct sequence spread spectrum
FFT	fast Fourier transform
FHT	fast Hadamard transform
HPA	high-power amplifier
IBO	input back-off
ICI	inter-carrier interference
ISI	inter-symbol interference
IDFT	inverse discrete Fourier transform
IFFT	inverse fast Fourier transform
LAN	local area network
MALD	majority logic decoding
MBPS	megabits per second
MDPSK	M-ary differential PSK
ML	maximum-likelihood
MLD	maximum-likelihood decoding

OBR	out-of-band radiation
OFDM	orthogonal frequency division multiplexing
OSD	ordered statistics decoding
OSR	oversampling ratio
PAPR	peak-to-average-power ratio
PSD	power spectral density
PSK	phase-shift keying
PTS	partial-transmit-sequence
QAM	quadrature amplitude modulation
RM	Reed-Muller
RMS	root mean square
SD	sphere decoding
SER	symbol error rate
SL	soft limiter
SLM	selected mapping
SNR	signal-to-noise ratio
SSPA	solid state power amplifier
STA	standard array of linear block codes
TWTA	travelling wave tube amplifier
WLAN	wireless local area network

Chapter 1

Introduction

Orthogonal frequency division multiplexing (OFDM) has gained increasing attention in the area of wireless communications. OFDM is presently incorporated in applications such as European HIPERLAN/2 and Japanese MMAC, and is part of the IEEE 802.11 standard [78].

Design and implementation of an OFDM transceiver is costly in terms of bandwidth efficiency and hardware resources if a straight-forward implementation is used. Advances in digital signal processing (DSP) have contributed to the design of OFDM based systems that have a simple implementation. One of the major contributions to the OFDM technology was the application of the fast Fourier transform (FFT) at both the transmitter and receiver.

The most desirable advantage of OFDM over single carrier systems is its superior performance in frequency selective fading channels. In OFDM, parallel transmission of high-rate signals over lower rate streams makes transmission less susceptible to corruption in the multi-path environment. However, OFDM signals consist of a large number of independent modulated subcarriers that can result in a high peak-to-average power ratio [69, 76]. If peak transmission power is limited (as is the case in practical applications) then average power

transmission in OFDM systems is reduced compared to systems with constant power modulations. The transmitted signal also has to pass through a high-power amplifier. Amplifiers enter the saturation region when they amplify high amplitude signals, and this causes intermodulation among adjacent sub-carriers. In order to prevent the resulting out-of-band radiation (OBR), it is imperative that amplifiers work in their linear region. This, together with the high instantaneous power of OFDM signals, force the receivers to be designed to accommodate substantially higher dynamic range.

A number of PAPR reduction techniques have been presented in the literature to deal with the high peak power of OFDM signals. These techniques fall into two major categories: distortionless techniques and PAPR reduction techniques with distortion. Each category will be discussed in detail in the following chapters. In this thesis, we focus on two distortionless techniques, namely, a recently proposed technique based on the standard array of linear block codes [97] and the use of block codes with limited PAPR.

1.1 Thesis Outline and Contributions

The thesis is organized as follows. Chapter 2 provides some background on OFDM technology. An overview of wireless LAN standards as well as definition of OFDM systems and their mathematical representation is presented. Following that, the features and drawbacks of OFDM are discussed and mathematical models of the communication channel as well as existing models for the nonlinearity of high-power amplifiers are reviewed. The statistics of PAPR and the mathematical tools for analytical study of the effect of nonlinearity in OFDM signals are provided. Finally, several existing PAPR reduction techniques are discussed. Employing block codes with guaranteed low PAPR

solves the problem of PAPR reduction in OFDM signals. We study Golay sequences [24], a well-known set of sequences with PAPR less than 3 dB [8,57] and their subsets [15,54] in detail throughout this chapter.

A drawback of using such codes is the high complexity of their corresponding maximum-likelihood (ML) decoders. ML decoding of a linear binary code is an NP-hard problem [86]. In Chapter 3, we propose an efficient maximum-likelihood decoding (MLD) algorithm for Golay sequences and provide simulation results for both AWGN and fading channels as well as for systems with amplifier non-linearities.

Following that, in Chapter 4, further improvements to the algorithm and the application of the proposed algorithm to both phase-shift keying and quadrature amplitude modulation is investigated and measures of complexity are developed. Finally, the proposed decoder is extended for M-ary differential phase-shift-keying OFDM (MDPSK-OFDM) receivers. Simulation results are provided to illustrate the comparison between the performance of the new and existing receivers in frequency selective fading channels.

In Chapter 5, we study the optimum design of a partial-transmit-sequence (PTS) scheme. An overview of the existing sub-optimum design techniques is provided and a new low-complexity optimizer is developed based on the idea of sphere decoding.

Finally, in Chapter 6, a recent technique for the reduction of PAPR based on a standard array of linear block codes is investigated in detail and its performance in non-ideal channels is evaluated. Also, coding techniques are employed to reduce the sensitivity of the BER performance of STA-based transceivers to channel distortion.

Chapter 7 concludes the thesis with a summary of the contributions.

Chapter 2

Literature Review

OFDM is a leading solution to the problem of multi-path fading in wireless communications. In this chapter we review the concepts behind OFDM and its mathematical representation. Various salient features and drawbacks of OFDM are also discussed. We then review the various mathematical models of the communication channel as well as existing models for the nonlinearity of high-power amplifiers. Further information regarding the statistics of PAPR and the mathematical tools for analytical study of the effect of nonlinearity in OFDM signals are then presented. Finally, existing PAPR reduction techniques are introduced and references for further study are provided.

2.1 Wireless LAN Standards

The introduction of standards for Wireless Local Area Network (WLAN) products has made WLANs one of the most dynamic branches of the communications industry. These products are mainly based on the IEEE 802.11b standard and are faster, lower in cost and simpler to use than the previous generation products. As per the design of IEEE 802.11b standard, most of the WLAN products communicate through wireless links at or up to 11 megabits per-

second (Mbps) data rates. The IEEE 802.11b standard, popularly known as 'Wi-Fi', specifies operation in the 2.4 GHz band using direct sequence spread spectrum (DSSS) technology.

In 1999, the IEEE approved two new WLAN standards known as IEEE 802.11a and IEEE 802.11g which could deliver higher speeds, up to 54 Mbps, to WLAN users. IEEE 802.11a transfers the data with 54 Mbps using OFDM technology at 5 GHz. However, since DSSS is easier to implement than OFDM, IEEE 802.11b products appeared on the market first. In early 2001, the FCC announced new rules allowing additional applications in the 2.4 GHz range. This allowed IEEE to extend IEEE 802.11b to support higher data rates, resulting in the IEEE 802.11g standard. It defines new data rate, up to 54 Mbps, at 2.4 GHz using OFDM, while still being backward compatible with 802.11b at speeds up to 11 Mbps using DSSS.

2.1.1 802.11a: High-Speed, High Capacity in the 5 GHz Band

By using OFDM modulation in 5 GHz band, the IEEE 802.11a standard offers two major benefits over IEEE 802.11b: it speeds up the data transfer rate per channel (from 11 Mbps to 54 Mbps) and it increases the number of non-overlapping channels. It also offers higher total bandwidth in the 5 GHz band compared to the available total bandwidth in the 2.4 GHz band (300 MHz versus 83.5 MHz). Therefore, an IEEE 802.11a-based WLAN can inherently support more simultaneous users without any conflict. However, despite the potential achievements of IEEE 802.11a, it has some drawbacks in terms of compatibility and range. IEEE 802.11a and IEEE 802.11b products are not compatible due to the fact that they are designed to operate in different frequency bands. However, both standards can certainly co-exist and operate in

the same physical space and share network resources. Another inherent bottleneck of IEEE 802.11a is that it offers a relatively shorter range. A larger number of IEEE 802.11a access points are generally needed to cover the same area.

2.1.2 802.11g: High-Speed in the 2.4 GHz Band

The IEEE 802.11g standard brings the benefits of higher speeds, while maintaining backward compatibility with existing IEEE 802.11b equipment. An IEEE 802.11g network card, for example, will work with an 802.11b access point and an IEEE 802.11g access point will work with IEEE 802.11b network cards at speeds up to 11 Mbps. IEEE 802.11g offers operation in the same 2.4 GHz frequency band and with the same DSSS transmission as 802.11b at speeds up to 11 Mbps, while simultaneously adding more efficient OFDM modulation types at higher speeds. The draft standard also specifies optional modulation types such as complementary-code-keying (CCK).

CCK was originally defined in [81] and later voted in at the July 1998 IEEE 802.11 conference [77]. CCK is a special case of the more general Golay sequences introduced originally in [24]. Let $\varphi_1, \cdots, \varphi_4$ represent four phases conveying the data bits. The CCK code is obtained according to the following equation

$$C = \left\{ e^{j(\varphi_1+\varphi_2+\varphi_3+\varphi_4)}, e^{j(\varphi_1+\varphi_3+\varphi_4)}, e^{j(\varphi_1+\varphi_2+\varphi_4)}, -e^{j(\varphi_1+\varphi_4)}, \right. \\ \left. e^{j(\varphi_1+\varphi_2+\varphi_3)}, e^{j(\varphi_1+\varphi_3)}, -e^{j(\varphi_1+\varphi_2)}, e^{j(\varphi_1)} \right\} \tag{2.1}$$

The three phases $\varphi_2, \varphi_3, \varphi_4$ define all possible different codes of length 8 and φ_1 offers an extra phase rotation to the codeword. Note that φ_1 can be differentially encoded across successive codewords. This feature allows the compatibility of the link with the 1 and 2 Mb/s DSSS differential phase encoding when

each of the four phases represent 2 bits of information. Since the codeword rate is 1.375 MHz, a 5.5 Mb/s data rate is achieved when each of the four phases contain one bit of information.

2.2 Orthogonal Frequency Division Multiplexing

OFDM divides the communication channel into parallel sub-channels and splits the high-rate data into those sub-channels. An OFDM symbol consists of n sub-carriers spaced by frequency distance Δf. All sub-carriers are mutually orthogonal within a time interval of length $T = \frac{1}{\Delta f}$. Consider the k-th data vector $\mathbf{D}_k = \{D_{k,0}, D_{k,1}, \cdots, D_{k,n-1}\}$. The OFDM signal of $\mathbf{D}_k$ is constructed by adding together n modulated data symbols with frequencies $f_0 + i\Delta f$ ($i = 0, 1, \cdots, n-1$), where f_0 is the carrier frequency of the transmission and Δf is the bandwidth of each sub-channel. The k-th OFDM block is formed as [65]

$$x_k(t) = \frac{1}{\sqrt{n}} \sum_{i=0}^{n-1} D_{k,i} \exp(j2\pi(f_0 + i\Delta f)t) g_i(t - kT) \tag{2.2}$$

where $g_i(t)$ is the pulse shaping applied to each subcarrier. The total continuous time signal $x(t)$ can be represented as

$$x(t) = \frac{1}{\sqrt{n}} \sum_{k=0}^{\infty} \sum_{i=0}^{n-1} D_{k,i} \exp(j2\pi(f_0 + i\Delta f)t) g_i(t - kT). \tag{2.3}$$

The statistics of $\mathbf{D}_k$ are assumed to be constant in different blocks. Therefore, it is sufficient to consider only one time slot of an OFDM signal; $D_{k,i}$ can thus

be replaced by D_i and we have

$$x(t) = \frac{1}{\sqrt{n}} \sum_{i=0}^{n-1} D_i \exp(j2\pi(f_0 + i\Delta f)t) \qquad 0 \leq t < T. \tag{2.4}$$

Implementation of an OFDM system in continuous time requires several sinusoidal generators and coherent demodulators. This makes OFDM systems complicated and expensive. However, representation of OFDM signals in the discrete-time domain significantly reduces system complexity and makes them easier to implement. The discrete-time representation of OFDM signals can be obtained by properly sampling the continuous-time OFDM signal. Since the total bandwidth of the OFDM signal is $B = n \cdot \Delta f$, the signal should be sampled at $\Delta t = \frac{1}{B} = \frac{1}{n\Delta f}$ for complete recovery of the original signal from its samples. Therefore, the discrete time samples can be represented as

$$x_k = \frac{1}{\sqrt{n}} \sum_{i=0}^{n-1} D_i e^{j2\pi ik/n} \qquad k = 0, 1, \cdots, n-1. \tag{2.5}$$

Eqn. (2.5) is the inverse discrete Fourier transform (IDFT) of the input data D_i and can efficiently be implemented using inverse fast Fourier transform (IFFT) algorithms.

Data symbols D_i can be selected from any modulation scheme such as phase-shift keying (PSK) or quadrature amplitude modulation (QAM). Let $\mathbb{Z}_q = \{0, 1, \cdots, q-1\}$ where $q = 2^h$ for some integer h. The q-PSK constellation is given as

$$\mathcal{Q}_{q-PSK} = \left\{ \xi^k | \xi = e^{\frac{j2\pi}{q}}, k \in \mathbb{Z}_q, j = \sqrt{-1} \right\}. \tag{2.6}$$

The q-QAM constellation is given as

$$\mathcal{Q}_{q-QAM} = \{[\pm(2k_1+1) \pm j(2k_2+1)], k_1, k_2 \in \{0, 1, \cdots, \log_2 q - 2\}\} \quad (2.7)$$

2.3 OFDM Over Wireless Channels

The transmitter output signal goes through a communication channel before reaching the receiver. In practice, the channel introduces distortion in both amplitude and frequency of the signals. A communication channel in its simplest form corrupts the signal by adding white Gaussian noise to the signal. A more realistic model for a wireless communication channel includes multi-path fading. A signal propagating through the wireless channel arrives at the receiver through different paths, referred to as multi-paths [56]. Let $x(t)$ be the input signal defined in (2.4). The output of the multi-path channel is the waveform

$$r(t) = x(t) \star c(t) + w(t) \quad (2.8)$$

where $c(t)$ is the impulse response of the channel, $\star$ represents convolution and $w(t)$ is the noise component [58].

OFDM regards the multi-path frequency selective fading channel as a set of parallel flat fading channels with frequency non-selective fading. Therefore, OFDM simplifies the problem of multi-path fading channels. However, OFDM introduces inter-symbol interference (ISI) and inter-carrier interference (ICI). ISI is the effect of previous OFDM symbols on the current symbol and ICI is the effect of one sub-channel on the other sub-channels in the OFDM symbol. Concatenating a proper guard interval time T_G to the beginning of each OFDM block could efficiently eliminate the ISI and ICI. Therefore, the received i-th

sub-channel output (after DFT demodulation) is

$$\hat{D}_i = D_i \rho_i + W_i \tag{2.9}$$

where D_i is the transmitted data, W_i is the additive noise component and ρ_i is the frequency response of the channel in the i-th subcarrier which can be represented as

$$\rho_i = H\left(\frac{2\pi i}{n}\right) = \sum_{k=0}^{v-1} c_k e^{-2\pi j i k/n}. \tag{2.10}$$

where c_k denotes the k-th multipath component and v is the length of the sampled channel impulse response. Typically, each c_k (also called a tap) is modelled as a complex Gaussian random variable.

Note that (2.10) is analogous to the output of a single-carrier scheme in flat fading. The performance of OFDM in the frequency selective fading channel is therefore similar to that of a single-carrier scheme with flat fading [58]. In order to enhance the BER performance of the OFDM system different channel coding techniques may be employed.

2.3.1 Channel model for frequency selective fading channels

Different models for fading channels such as fast fading and slow fading channels are widely used in the literature depending on the rate of variation of the channel statistics with respect to the OFDM symbol duration. In this thesis, we use the typical channel profiles of indoor office areas with moderate delay spread, as is modelled in [49]. Each tap of the profile represents an instance of uncorrelated Rayleigh fading. Fig. 2.1 shows the average power versus the excess delay. The root mean square (rms) delay spread is 35 ns which is defined

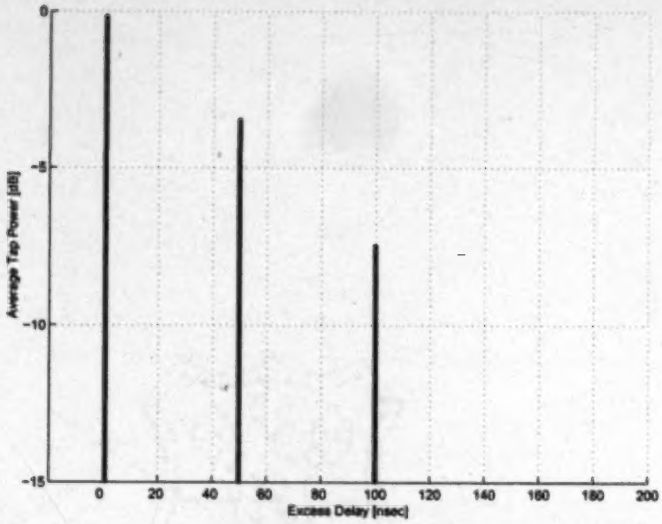

Figure 2.1: Typical channel profile for indoor office area with moderate delay spread

as

$$\tau_{\text{rms}} = \sqrt{\frac{\int |c(\tau)|^2 . (\tau - \bar{\tau})^2 \, d\tau}{\int |c(\tau)|^2 \, d\tau}} \tag{2.11}$$

with

$$\bar{\tau} = \frac{\int |c(\tau)|^2 . \tau d\tau}{\int |c(\tau)|^2 \, d\tau} \tag{2.12}$$

where $c(\tau)$ is the channel impulse response defined in (2.8).

2.4 Peak-To-Average-Power ratio

An inherent characteristic of OFDM signals is that they have amplitude variations with a large dynamic range. OFDM signals usually have peak-to-average-power ratio (PAPR) much greater than unity. This leads to a higher power consumption that is not tolerable in portable applications. Consider the OFDM

signal in (2.4). The PAPR of data vector $\mathbf{D}$ is defined as [31]

$$\text{PAPR}(\mathbf{D}) = \frac{\max\limits_{0 \le t < T} |x(t)|^2}{P_{av}} \tag{2.13}$$

where $|x(t)|^2$ represents the instantaneous power of the OFDM signal ($x(t)$) and P_{av} is the first order estimate of $\bar{P}$ (*i.e.* $P_{av} = E\{\bar{P}\}$). The root mean square (rms) magnitude of the OFDM signal can be evaluated as follows:

$$\bar{P} = \frac{1}{T}\int_{t=0}^{T} |x(t)|^2 dt = \frac{1}{n}\sum_{i=0}^{n-1} |D_i|^2. \tag{2.14}$$

The crest factor (CF) is also used to measure the variation of the OFDM signals. The crest factor is defined as

$$\text{CF}(\mathbf{D}) = \frac{\max\limits_{0 \le t < T} |x(t)|}{\sqrt{P_{av}}} \tag{2.15}$$

Therefore, the CF is the square root of PAPR. In the study of OFDM signals, statistics of the PAPR are expressed in terms of its complementary cumulative distribution function (CCDF). Note that λ% PAPR indicates the probability that PAPR exceeds $\frac{\lambda}{100}$.

2.4.1 Definition of PAPR

The PAPR of an OFDM signal can be accurately obtained from its continuous-time representation. In practice, OFDM systems are implemented in the discrete-time domain using FFT modules. The resulting OFDM samples are hence the Nyquist-rate samples of the OFDM signal. In the receiver, the continuous-time signal is reconstructed by filtering the discrete OFDM samples. However, the peak value computed from the discrete samples may not

coincide with that of the continuous-time signal [69]. In order to accurately compute the PAPR, oversampling is used. The OFDM samples in (2.5) are obtained with sample rate nL where L ($L > 1$) is a positive integer [44,73–75]. Therefore, $L-1$ zeros are padded after each original data symbol to form the new data vector $\mathbf{D}^L = \{D_0^L, \cdots, D_{nL-1}^L\}$ where

$$D_i^L = \begin{cases} D_{i/L} & i \mod L = 0 \\ 0 & \text{otherwise} \end{cases} \tag{2.16}$$

for $0 \leq i < nL$. The oversampled signal is represented as

$$x_k^L = \frac{1}{\sqrt{n}} \sum_{i=0}^{nL-1} D_i^L e^{j2\pi ik/nL} \qquad k = 0, 1, \cdots, nL-1. \tag{2.17}$$

Accordingly, the PAPR of the discrete time symbols x_k^L is

$$\text{PAPR}_L(\mathbf{D}) = \frac{\max\limits_{k\in[0,nL)} \left|x_k^L\right|^2}{E\left\{\left|x_k^L\right|^2\right\}}. \tag{2.18}$$

Note that when $L = 1$, (2.18) corresponds to the PAPR approximation for the Nyquist-rate sampling. Also as $L \to \infty$, (2.18) yields (2.13).

2.4.2 PAPR Approximation Using Oversampling

Determining the relationship between the PAPR of the oversampled OFDM signal and the continuous OFDM signal is a challenging problem. This problem has extensively been discussed in [71, 89]. A new bound is proposed for the peak of the continuous envelope of an OFDM signal in [69]. In this section, we outline this approach and review the results.

Consider the base-band equivalent of the OFDM signal defined in (2.4)

(i.e. $f_0 = 0$) with $\theta = 2\pi t/T$ for mathematical simplicity. We have

$$x(\theta) = \frac{1}{\sqrt{n}} \sum_{i=0}^{n-1} D_i e^{j\theta i}, \qquad 0 \le \theta < 2\pi. \tag{2.19}$$

Let θ_0 be defined as $|x(\theta_0)| = \max_{0 \le \theta < 2\pi} |x(\theta)|$. It is shown in [69] that for any real value of $\beta > 0$ and for all θ in the interval $[\theta_0 - 1/n\sqrt{(2\beta)/(\beta+1)}, \theta_0 + 1/n\sqrt{(2\beta)/(\beta+1)}]$,

$$|x(\theta)| > \sqrt{\frac{1}{\beta+1}} |x(\theta_0)|. \tag{2.20}$$

Using (2.20), an upper bound was obtained for the maximum of the continuous signal in terms of the maximum of the oversampled values [69]. Let k be a real parameter greater than $\pi/\sqrt{2}$. The maximum of $|x(\theta)|$ is bounded by the maximum of its kn samples on the unit circle by

$$\max_{0 \le \theta < 2\pi} |x(\theta)| < \sqrt{\frac{k^2}{k^2 - \pi^2/2}} \max_{1 \le p < kn} \left| x\left(\frac{2\pi p}{kn}\right) \right| \tag{2.21}$$

Clearly, when k is large, the maximum of the oversampling OFDM signal approaches that of the continuous OFDM signal. Let us define θ_p such that $e^{j\theta_p}$ be the primitive kn roots of unity as:

$$\theta_p = \frac{2\pi p}{kn}, \qquad p \in \{1, 2, \cdots, kn\}. \tag{2.22}$$

Inequality (2.21) shows that for any $k > \pi/\sqrt{2}$ where kn is an integer, we have the following bound on the CCDF of the PAPR of $x(\theta)$

$$\Pr\{PAPR > \lambda\} < \Pr\left\{ \max_{1 \le p < kn} \frac{|x(\theta_p)|^2}{P_{av}} > \lambda \left(1 - \frac{\pi^2}{2k^2}\right) \right\}. \tag{2.23}$$

As mentioned before, all D_i are independently and uniformly selected from

a constellation, therefore, $x(\theta_p)$ is a Gaussian random variable with variance P_{av}. A union bound can be used to calculate the inequality (2.23) as

$$\begin{aligned}
&\Pr\left\{\max_{1\le p<kn}\frac{|x(\theta_p)|^2}{P_{av}} > \lambda\left(1-\frac{\pi^2}{2k^2}\right)\right\} \\
&\qquad = \Pr\left\{\exists p\in\{1,\cdots,kn\} : \frac{|x(\theta_p)|^2}{P_{av}} > \lambda\left(1-\frac{\pi^2}{2k^2}\right)\right\} \\
&\qquad \le kn\Pr\left\{\frac{|x(\theta)|^2}{P_{av}} > \lambda\left(1-\frac{\pi^2}{2k^2}\right)\right\} \\
&\qquad = kne^{\lambda\left(1-\frac{\pi^2}{2k^2}\right)}. \qquad (2.24)
\end{aligned}$$

The new bound is valid for every $k > \pi/\sqrt{2}$ [69]. A tighter bound can be obtained by minimizing (2.24) over k. Differentiating with respect to k results in the optimum oversampling rate k_{opt} given as

$$\frac{\pi^2}{k_{opt}^2}\left(1-\frac{\pi^2}{k_{opt}^2}\right) = \frac{1}{2\lambda} \qquad (2.25)$$

where $k_{opt}n$ is an integer.

2.4.3 Statistics of PAPR

In a simplistic model of an OFDM system, data symbols D_i are assumed to be statistically independent random variables chosen from a known modulation alphabet (*i.e.* PSK or QAM). These symbols construct the OFDM signal, which has a high dynamic range in amplitude. Although these signals potentially can have high peak power, the rate of occurrence of these peaks is low. Therefore, it might not be optimum to design the transceiver for the highest dynamic range of OFDM signals. In order to approximate the dynamic range required in the design of transceivers, a statistical distribution of the peak power of OFDM signals has to be determined. Reference [79] has estimated

the statistical distribution of an OFDM signal based on the assumption that the baseband OFDM signal converges to a complex Gaussian random process as the number of sub-carriers increases. The resulting approximation does not match with computer simulations [72]. This difference arises because the approximation approach is valid for the peak OFDM samples, but not necessarily for the maximum-peak of the continuous OFDM. Oversampling could be used to accurately estimate the maximum-peak of the OFDM symbols. However, the assumption that the OFDM samples are mutually uncorrelated no longer holds. An empirical approximation is proposed in [80] where the distribution of the oversampling case is approximated with the distribution of an OFDM signal with αn ($\alpha > 1$) subcarriers without oversampling. As a result, the CCDF of the peak power is approximated as [80]

$$\Pr\left(\max_{0\leq k<n} p_k < p\right) = \left(1 - e^{-p}\right)^{\alpha n} \tag{2.26}$$

where p_k is the k-th peak of the OFDM signal. Reference [80] shows that $\alpha = 2.8$ is a practical approximation for (2.26).

The exact analytical expression for the distribution of PAPR in OFDM signals as well as its simplified approximations are introduced in [52]. Assuming that the data symbols in (2.4) are wide-sense stationary Gaussian random processes, the OFDM signal is a stationary band-limited Rayleigh process. Distribution of the peak of random signals is investigated in [63,64] as well as derivation of the distribution of the peak of Gaussian and Rayleigh random processes. The distribution of an arbitrary peak in an OFDM signal and the analytical expression for the CCDF of an OFDM signal which are proposed

in [52] are as follows:

$$\Pr\left(\max_{0\le k<n} p_k < p\right) \approx \left(1 - \frac{\overline{n}_p(p)}{0.64n}\right)^{0.64n} \tag{2.27}$$

where p_k is defined as in (2.26) and where

$$\overline{n}_p(\alpha) = \frac{4n}{\sqrt{15\pi}} \int_\alpha^\infty u^2 \int_0^\infty e^{-(\Phi^2+1)u^2} \cdot \left\{ e^{-\frac{3}{4}(\Phi^2-1)^2 u^2} - \frac{\sqrt{5\pi}}{2}\left(\Phi^2-1\right) u \cdot \operatorname{erfc}\left(\frac{\sqrt{5}}{2}\left(\Phi^2-1\right)u\right)\right\} d\Phi du. \tag{2.28}$$

These results are based on the assumption that the data symbols are stationary and are statistically independently Gaussian distributed.

2.5 High Power Amplifier and Nonlinearity

Multi-carrier signals in general and OFDM signals in particular are more susceptible to nonlinearity of the transceiver than single carrier modulated systems. The source of nonlinearities in practical communication systems include nonlinearity in the IDFT and DFT blocks due to limited word length, signal clipping due to the A/D and D/A conversion, and nonlinearity of the high-power amplifiers. Nonlinearity results in inter-carrier interference which degrades the performance of the transceiver. However, due to the high PAPR of OFDM signals, the majority of degradation is caused by high-power amplifiers. Therefore, it is helpful to have a precise model for the characteristics of the high-power amplifiers.

2.5.1 Nonlinearity Models

A high power amplifier is usually modelled as a memoryless device [66]. The input-output relationship is given by

$$f(r) = h(r)e^{j\theta(r)} \tag{2.29}$$

where r is the input amplitude, $\theta(r)$ is the output phase and $h(r)$ is the output amplitude. Let

$$x(t) = r(t) \cdot e^{j\phi(t)} \tag{2.30}$$

represent the input of the nonlinear amplifier. Hence, the complex envelope of the output signal can be written as

$$\begin{aligned} y(t) &= R(t) \cdot e^{j\Phi(t)} \\ &= h[r(t)] \cdot e^{j(\theta(r(t))+\phi(t))} \\ &= f[r(t)] \cdot e^{j\phi(t)} \end{aligned} \tag{2.31}$$

where $R(t)$ shows the effect of nonlinearity on the amplitude $r(t)$ and $\Phi(t)$ shows the effect of nonlinearity on the phase $\phi(t)$ of the input signal.

There are three models for high-power amplifiers which are commonly used in the literature: the Soft-Limiter (SL), the Solid State Power Amplifier (SSPA) and the Travelling Wave Tube Amplifier (TWTA) [20].

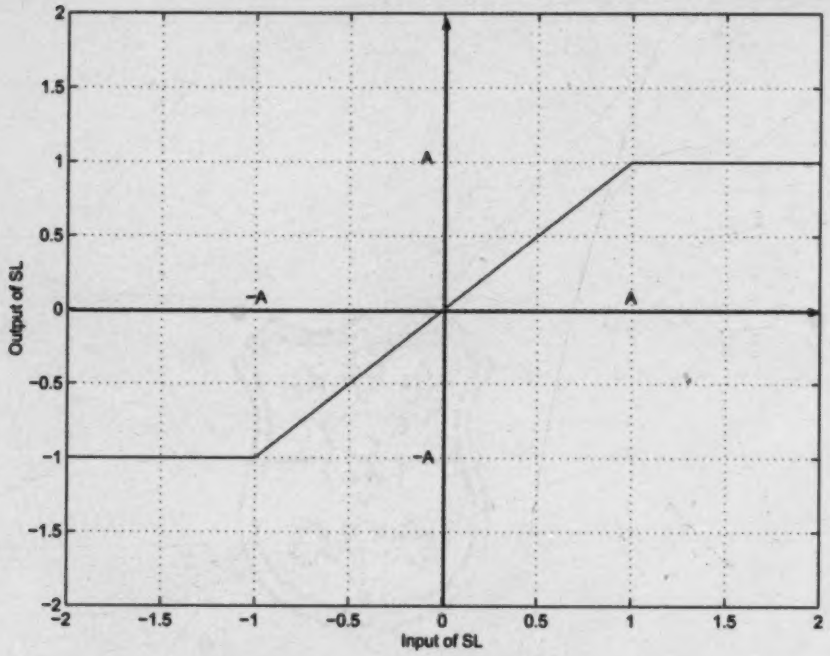

Figure 2.2: Amplitude (AM/AM) characteristic of a soft limiter

Soft Limiter

The amplitude (AM/AM) and phase (AM/PM) nonlinear characteristics of a soft limiter can be expressed as

$$R(t) = \begin{cases} r(t) & r(t) \leq A \\ A & r(t) \geq A \end{cases} \tag{2.32}$$

and

$$\Phi(t) = \phi(t) \tag{2.33}$$

where A denotes the saturation limit of the amplifier as shown in Fig. 2.2. This model is an optimistic model for the HPA nonlinearity and is accurate only if proper pre-distortion is employed for linearization.

Travelling Wave Tube Amplifier(TWTA)

The effect of nonlinearity on the amplitude of the input signal (AM/AM conversion function) for a TWTA is given by [68]

$$R(t) = \frac{2Ar(t)}{1 + \left(\frac{r(t)}{A}\right)^2} \tag{2.34}$$

where $r(t)$ is the input signal and A is the saturation level of the amplifier. As well, the relation between the amplitude of the input signal and the phase of the output signal (AM/PM conversion function) is given by

$$\Phi(t) = \phi(t) + \frac{\pi}{3}\frac{r(t)}{r^2(t) + 4A^2}. \tag{2.35}$$

This model gives a maximum output signal of A, as shown in Fig. 2.3.

Solid State Power Amplifier (SSPA)

The amplitude and phase functions for this type of amplifier can be modelled as [61]

$$\begin{aligned} R(t) &= \frac{r(t)}{[1 + \left(\frac{r(t)}{A}\right)^{2p}]^{\frac{1}{2p}}}, \\ \Phi(t) &= \phi(t). \end{aligned} \tag{2.36}$$

Parameter p controls the smoothness of the linear region in the characteristic curve for the HPA, as shown in Fig. 2.4. As a special case, when $p \longrightarrow \infty$ the characteristic of SSPA is similar to that of the SL.

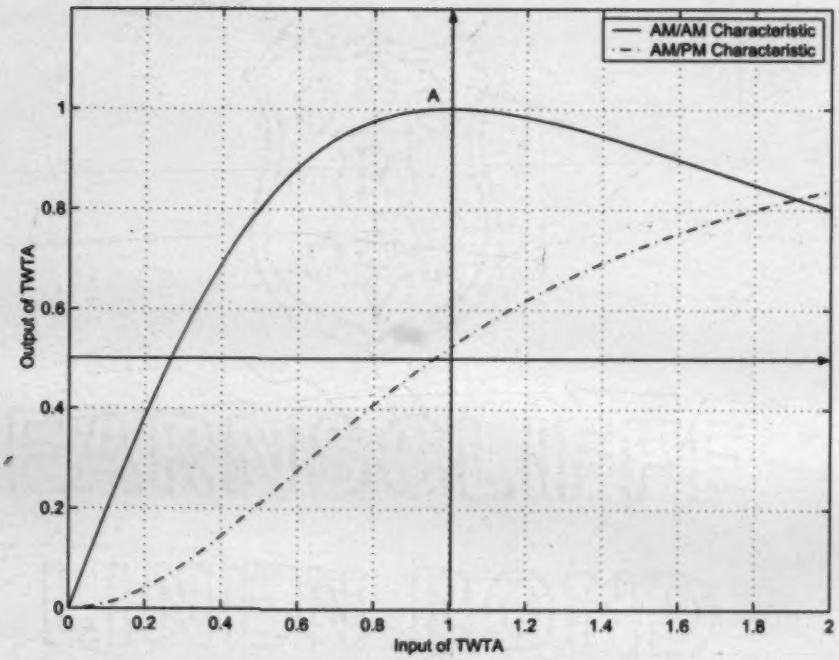

Figure 2.3: Amplitude (AM/AM) and phase (AM/PM) characteristics of TWTA

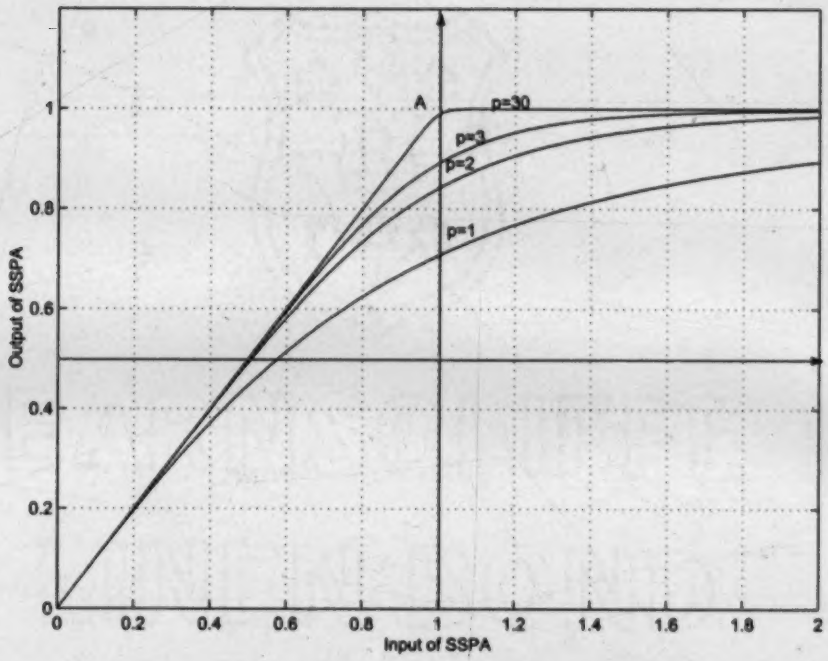

Figure 2.4: Amplitude (AM/AM) characteristic of SSPA

2.5.2 Theoretical Performance Analysis Of OFDM Systems In The Existence Of Nonlinearity

An expression for the bit error rate of an OFDM system with a nonlinear amplifier may be derived using the Bussgang theorem, which relates the output correlation to the input correlation as [6]

$$\mathcal{R}_{yy}(\tau) = |\alpha|^2 \cdot \mathcal{R}_{xx}(\tau) + \mathcal{R}_{ww}(\tau). \tag{2.37}$$

In (2.37) w represents the distorted part of the output signal y, x represents the input signal and the complex coefficient α is given by [6]

$$\begin{aligned} \alpha &= \frac{\mathcal{R}_{yx}(0)}{\mathcal{R}_{xx}(0)} \\ &= \frac{1}{2\sigma^2} \int_0^\infty f(r) \cdot r \cdot p(r) dr \end{aligned} \tag{2.38}$$

where σ^2 is the variance of the OFDM symbols. In (2.38) the numerator corresponds to the complex input-output cross-correlation function, $f(r)$ corresponds to the nonlinearity distortion function and $p(r)$ corresponds to the distribution function of the input envelope. In the case where the distribution of the input signal is Gaussian, $p(r)$ represents the Rayleigh distribution. The signal to nonlinear-noise ratio can be expressed as

$$\begin{aligned} (SNR)_d &= \frac{|\alpha|^2 \cdot \mathcal{R}_{xx}(0)}{\mathcal{R}_{ww}(0)} \\ &= \frac{|\alpha|^2 \cdot 2\sigma^2}{\mathcal{R}_{yy}(0) - |\alpha|^2 \cdot 2\sigma^2}. \end{aligned} \tag{2.39}$$

An accurate expression for the output correlation $\mathcal{R}_{yy}(\tau)$ in terms of the input correlation is derived in [6]

$$\begin{aligned}\mathcal{R}_{yy}(\tau) &= \sum_{i=0}^{\infty} c_i \left[\frac{\mathcal{R}_{xx}(\tau)}{2\sigma^2}\right]^{2i+1} \\ &= \frac{c_0}{(2\sigma^2)}\mathcal{R}_{xx}(\tau) + \sum_{i=1}^{\infty} c_i \left[\frac{\mathcal{R}_{xx}(\tau)}{2\sigma^2}\right]^{2i+1}\end{aligned} \tag{2.40}$$

In (2.40), parameter c_i can be computed according to [6] as:

$$c_i = \frac{1}{2\sigma^2}\frac{1}{i+1} \cdot \left\| \int_0^{\infty} f(r) \cdot \frac{r^2}{\sigma^2} \cdot e^{r^2/2\sigma^2} \cdot L_i^1\left(\frac{r^2}{2\sigma^2}\right) dr \right\|^2 \tag{2.41}$$

where $L_i^k(x)$ is the Laguerre function expressed by

$$L_i^{(k)}(x) = \frac{x^{-k}e^x}{i!}\left(\frac{d}{dx}\right)^i \left(x^{i+k} \cdot e^{-x}\right). \tag{2.42}$$

Theoretical analysis and performance evaluation in nonlinear fading channels is investigated in [5] where analytical symbol-error-rate (SER) in Rayleigh and Rice fading channels is derived.

2.6 PAPR Reduction Techniques

The potentially high peak-to-average power ratio (PAPR) of OFDM is a significant drawback of these systems. Reduction of PAPR is a challenging problem. A large body of research is available in the literature and several PAPR reduction techniques have been developed to overcome the problem of high PAPR with reasonable complexity. This section reviews three classes of PAPR reduction techniques: signal distortion techniques, approaches involving probabilistic multiple signalling, and block coding for PAPR reduction.

2.6.1 Signal Distortion Techniques

Signal distortion techniques reduce PAPR by distorting the transmitted signal before it passes through high-power amplifiers. The distortion can be as simple as clipping the signal peaks [1,12,43,50,51,53,87,90] or companding (pre/post distortion) [83,84]. These techniques significantly reduce PAPR. However, the distortions will degrade the BER.

Clipping and Filtering

Distorting the OFDM signal by clipping and filtering is proposed in [90]. Since signals with large PAPR occur rarely, clipping the signal based on the characteristics of the high-power amplifier (*i.e.* saturation level) can prevent transmission of high PAPR signals. The idea is to clip the signal with respect to a certain clipping level before transmission [12]. Let x_{clip} be the clipping threshold. The clipping level in dB can be defined as

$$CL = 20 \log_{10} x_{\text{clip}}. \tag{2.43}$$

The signal x is clipped according to the following inequalities

$$T(x) = \begin{cases} x & |x| \leq x_{\text{clip}} \\ x_{\text{clip}} \cdot e^{j \arg(x)} & |x| > x_{\text{clip}} \end{cases}. \tag{2.44}$$

Clipping causes distortion in the signal which can be viewed as an additional source of noise with components in both in-band and out-of-band spectra [50]. The latter can be eliminated by filtering, while the former cannot be reduced by filtering. If Nyquist-rate filtering is used, all of the noise falls in the OFDM signal band and cannot be removed by filtering. However, oversampling shapes a portion of the noise outside the signal band which can later be removed by

filtering after clipping. Filtering of the severely clipped signal can preserve the spectral efficiency of the system and hence improves the the BER performance but may introduce peak power regrowth. To reduce the overall peak regrowth, repeated clipping-and-filtering is proposed [3]. Reference [51] introduced the combined Nyquist rate filtering and adaptive symbol selection and analyzed the theoretical BER of the scheme.

The impact of clipping on PAPR reduction capability and channel capacity is studied in [53]. The effects of clipping on the performance of OFDM systems is investigated in [1] for a frequency selective fading channel. It is argued that the notch in the channel frequency response partly eliminates the clipping noise and enhances the signal to noise ratio.

Companding

Another distortion technique for the reduction of PAPR is the use of a compander [41,83–85,91]. Companding is typically used for speech signal transmission in order to optimize the required number of bits/sample for analog to digital conversion. Speech signals with extreme amplitudes occur rarely. Similarity between the speech signals and OFDM signals is the motivation to apply the companding technique for the PAPR reduction of OFDM systems [92,93].

$$x_c = A\frac{x \cdot \ln\left[1+\mu\left|\frac{x}{A}\right|\right]}{|x| \cdot \ln(1+\mu)} \tag{2.45}$$

where x_c is the companded signal, x is the input signal and μ is the companding parameter. The use of the μ-law companding technique is studied extensively in [83,84]. The OFDM signal x is distorted according to (2.45). On the receiver side, the received OFDM signal r is expanded before demodulation to retrieve

the original OFDM signal r_e according to [83]

$$r_e = A \cdot \frac{\exp\left\{\frac{r}{A \cdot \mathrm{sgn}(r)} \ln(1+\mu)\right\} - 1}{\mu \cdot \mathrm{sgn}(r)}. \tag{2.46}$$

The effect of companding on the BER performance of OFDM systems in AWGN is studied in [83] and it is shown that reasonable symbol error rates (SER) could be achieved by choosing a proper companding coefficient. Moreover, the SER of the companded OFDM signal is theoretically analyzed and compared to that of ordinary OFDM in [91]. Finally, a novel nonlinear companding transform technique has recently been proposed in [41] that effectively reduces the PAPR of the OFDM signal by adjusting the transformation parameters based on the statistics of the transmitted OFDM signals.

2.6.2 Probabilistic Multiple Signalling

Various probabilistic approaches are proposed in the literature [40] including selected mapping (SLM) [12, 35, 60, 96], partial transmit sequences (PTS) [33, 67, 75], interleaved OFDM, the sign design algorithm [70] and the use of standard array of linear block codes (STA) [97]. In what follows, we review some of the existing probabilistic approaches for PAPR reduction. However, we postpone the review of the STA technique to a separate chapter for a more detailed investigation.

Selected Mapping

Selected mapping (SLM) is a relatively simple approach for the reduction of PAPR in OFDM systems [60]. Input data vectors $\mathbf{D} = \{D_0, \cdots, D_{n-1}\}$ are multiplied by M pseudo-noise vectors $\mathbf{P}^i = \{P_0^i, \cdots, P_{n-1}^i\}, i = 0, \cdots, M-1$ in the transmitter where P_k^i are phase coefficients (*i.e.* $P_k^i = e^{j\phi_k^i}, \phi_k^i \in [0, 2\pi)$).

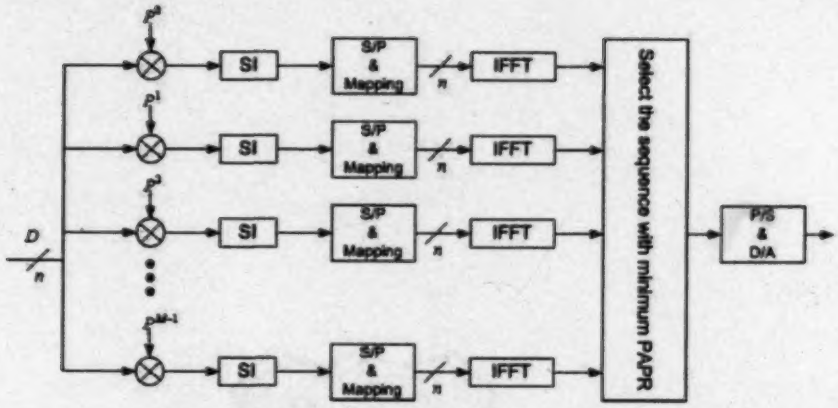

Figure 2.5: Block diagram of an OFDM transmitter with selected mapping

This will generate M OFDM symbols representing a given data vector $\mathbf{D}$. The sequence with the minimum PAPR is transmitted. Fig. 2.5 depicts a block diagram of selected mapping.

The performance of SLM, similar to other multiple signal generating techniques, depends on the number of multiple symbols generated. A lower bound on the achievable PAPR of the signal with respect to M is proposed in [40].

In order to transmit the information about which of the M pseudo-noise vectors is used for PAPR reduction, $\lceil \log_2 M \rceil$ additional bits need to be transmitted along with the data vector. These additional bits are called side information. However, a selected mapping technique is proposed in [9] which does not transmit any explicit side information to the receiver side. The data vector is concatenated with a set of label bits and the result is sent across a scrambler to generate a new set of signals with different PAPR characteristics. The SLM technique can also use the check-bits of the coded OFDM for PAPR reduction [27]. Therefore, both PAPR and BER reduction is achieved in this way. Moreover, distortion in the transmission of side information can be partly recovered. Finally, in [39] a blind SLM receiver was proposed to eliminate the

need for transmission of any side information across the channel.

Xin and Fair recently proposed a new PAPR reduction scheme [96] that employs guided scrambling in the SLM technique. Guided scrambling has been proposed for use in recording systems, digital data transmission, and the design of sequences with specific constraints such as zero-DC codes [17–19,94,95]. The use of guided scrambling performs close to the conventional SLM techniques but does not require transmission of explicit side information [96]. Finally, a low complexity implementation of SLM is proposed in [82].

Partial Transmit Sequence

Partial transmit sequence (PTS) is another multiple signal generation technique [12, 29, 30, 33, 67, 75]. In PTS, the input data of length n is partitioned into disjoint sub-blocks [12]. The IDFT of each sub-block is computed separately and combined to minimize the peak-to-average power ratio. Let $\mathbf{D} = \{D_0, \cdots, D_{n-1}\}$ be the input data. The data block $\mathbf{D}$ is divided into M disjoint subsets $\mathbf{D}^i = \{D_0^i, \cdots, D_{n/M-1}^i\}, i = 0, \cdots, M-1$ where

$$\mathbf{D} = \sum_{i=0}^{M-1} \mathbf{D}^i. \tag{2.47}$$

Sub-blocks are multiplied by pure rotations $b_i, i = 0, \cdots, M-1$ as shown in Fig. 2.6. PTS optimizes the values of rotation phases to minimize the PAPR of the following expression

$$\mathbf{d} = \sum_{i=0}^{M-1} b_i \mathbf{d}^i \tag{2.48}$$

where $\mathbf{d}$ and $\mathbf{d}^i$ are the IFFT of the sub-block vectors $\mathbf{D}$ and $\mathbf{D}^i$ respectively. Optimization of the rotation variables b_i has exponential complexity as the order of constellation or the value of M increases. Therefore, sub-optimal optimizations are investigated in the literature. An adaptive sub-optimal approach

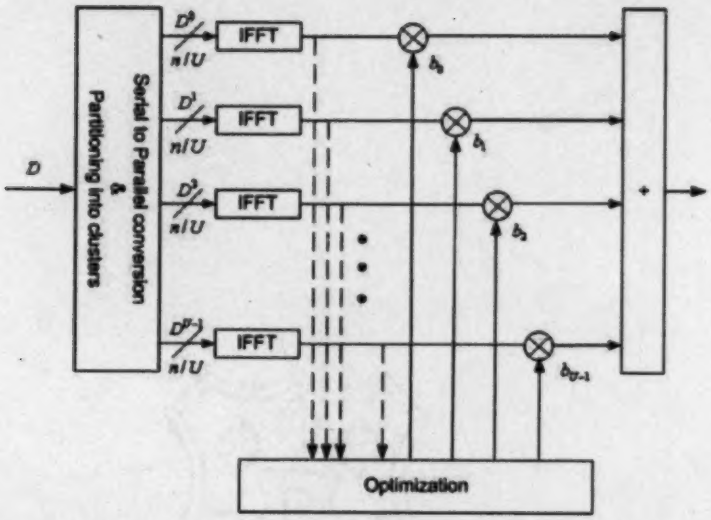

Figure 2.6: Block diagram of an OFDM transmitter using partial transmit sequence (PTS)

was introduced in [33] to optimize the phase factors in PTS with tolerable complexity. The idea is to stop the optimization when a solution with PAPR less than a certain level is found. Therefore, the optimization does not need to exhaustively search all the search space. A sub-optimal approach was proposed based on dual layered phase optimization [29,30] where the phase factors were categorized into two levels and separate optimization was performed on each level.

PTS also promises to reduce the large amplitude of MC-CDMA systems and low-complexity designs have been proposed [98].

Interleaved OFDM

One approach to generate multiple OFDM signals with the same information is to use interleavers [32, 34–37]. Fig. (2.7) shows the block diagram of an interleaved OFDM system. The input data is reordered according to

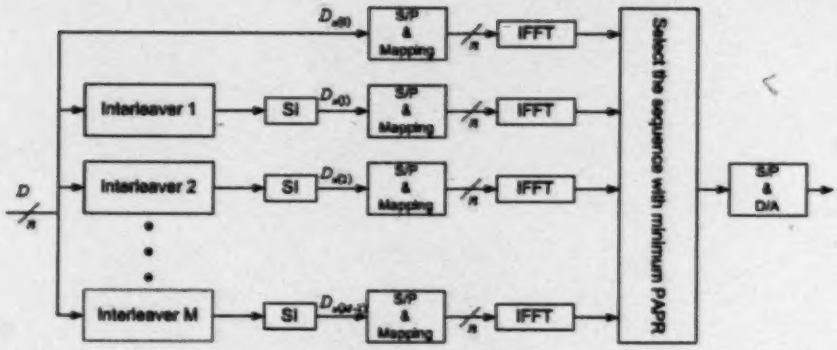

Figure 2.7: Block diagram of the interleaved OFDM transmitter

different permutations and the one with lowest PAPR is selected for transmission. Interleaving may be performed on either bits or on symbols. Let $\mathbf{D} = \{D_0, \cdots, D_{n-1}\}$ represent the data symbols. The permuted sequences are obtained according to

$$\mathbf{D}_{\pi_i} = \{D_{\pi_i(0)}, \cdots, D_{\pi_i(n-1)}\}\,,\ i = 0, \cdots, M-1 \tag{2.49}$$

where $\pi_i (i = 1, \cdots, M)$ are M distinct permutations of $\{0, 1, \cdots, n-1\}$. If the resulting M interleaved outputs $\mathbf{D}_{\pi_i}$ are uncorrelated, the theoretical CCDF of the PAPR of the interleaved OFDM signal can be derived [36–38] using (2.26) as

$$\Pr\left(\text{PAPR} > p\right) = \left(1 - \left(1 - \exp\left(-p\right)\right)^{\alpha n}\right)^M \tag{2.50}$$

Comparison between the distribution of PAPR obtained from theory (*i.e.* Eqn. (2.50)) and from simulation results for interleaved OFDM, as well as a new adaptive interleaving technique can be found in [38].

2.6.3 Block Coding

Block coding for PAPR reduction was initially proposed in [42] based on table look-up coding. The most comprehensive peak-reduction block-coding approach known to date is based on Golay sequences. The PAPR of a Golay sequence is at most 2 [8, 57]. Following Golay's seminal paper [24], a large number of researchers have investigated properties, recursive constructions, and existence results for Golay sequences. Davis and Jedwab [15] and Paterson [54] made important breakthroughs leading to explicit constructions of Golay sequences and showed that these sequences are cosets of the classical first-order Reed-Muller (RM) codes. For this reason, we use the terms Golay sequences and RM codes interchangeably. Golay-sequence codes for quadrature amplitude modulation are considered in [4, 11, 62].

Golay Sequences

Let us consider the OFDM signal in (2.4) where data symbols D_n use PSK modulation according to (2.6). Eqn. (2.4) can be rewritten as

$$x(t) = \frac{1}{\sqrt{n}} \sum_{i=0}^{n-1} \xi^{a_i} \exp(j2\pi(f_0 + i\Delta f)t) \qquad 0 \le t < T \qquad (2.51)$$

for $a_i \in \mathbb{Z}_q$. The PAPR of $x(t)$ is obtained using (2.13) where $P_{av} = 1$ for PSK modulation. The instantaneous power of the data vector $\mathbf{a} = (a_0, a_1, \cdots, a_{n-1})$ is obtained using $P_{\mathbf{a}}(t) = |x(t)|^2$ which is computed as

$$P_{\mathbf{a}}(t) = \frac{1}{n} \sum_{i_1=0}^{n-1} \sum_{i_2=0}^{n-1} \xi^{a_{i_1} - a_{i_2}} \exp(j2\pi(i_1 - i_2)\Delta f t) \qquad 0 \le t < T \qquad (2.52)$$

Letting $u = i_2 - i_1$ (2.52) gives

$$P_{\mathbf{a}}(t) = 1 + \frac{1}{n}\sum_{u\neq 0}\sum_{i_1=0}^{n-1} \xi^{a_{i_1}-a_{i_1+u}} \exp(-j2\pi u\Delta f t). \qquad 0 \le t < T \qquad (2.53)$$

The aperiodic autocorrelation of **a** is defined as

$$C_{\mathbf{a}}(u) = \sum_{k} \xi^{a_k - a_{k+u}}. \qquad (2.54)$$

Hence, (2.53) can be written in terms of the aperiodic autocorrelation as

$$P_{\mathbf{a}}(t) = 1 + \frac{1}{n}\sum_{u\neq 0} C_{\mathbf{a}}(u) \exp(-j2\pi u\Delta f t). \qquad 0 \le t < T \qquad (2.55)$$

Two sequences **a** and **b** are called a Golay complementary pair if the following condition holds:

$$C_{\mathbf{a}}(u) + C_{\mathbf{b}}(u) = 0 \qquad \forall u \neq 0. \qquad (2.56)$$

Let the set of all Golay sequences of length n be denoted by $GS(n)$. Rewriting (2.55) for **b** and adding the result to (2.55) gives

$$P_{\mathbf{a}}(t) + P_{\mathbf{a}}(t) = 2 + \frac{1}{n}\sum_{u\neq 0} [C_{\mathbf{a}}(u) + C_{\mathbf{a}}(u)] \exp(-j2\pi u\Delta f t) \qquad 0 \le t \le T \qquad (2.57)$$

According to (2.56) if **a** and **b** are a Golay pair then (2.57) is simplified to

$$P_{\mathbf{a}}(t) + P_{\mathbf{b}}(t) = 2 \qquad (2.58)$$

and since both instantaneous power terms are positive, one can conclude that

$$P_{\mathbf{a}}(t) \le 2. \qquad (2.59)$$

Therefore, the PAPR of Golay sequences is limited to 2 (3 dB).

Davis and Jedwab [15] appear to give the first explicit construction for $GS(2^m)$ (m a positive integer). A notable result of their work is that for $\mathbf{c} \in GS(n)$, $n = 2^m$, they proved that there exists $d_k \in \mathbb{Z}_{2^h}, k = 0, 1, \cdots, m$ such that

$$c_i = \sum_{k=1}^{m} d_k i_k + d_0 + \underbrace{2^{h-1} \sum_{k=1}^{m-1} i_{\pi(k)} i_{\pi(k+1)}}_{\text{coset term}}, \qquad i = 0, 1, \cdots, n-1, \qquad (2.60)$$

where $[i_1, i_2, \cdots, i_m]$ is the binary expansion of the integer i such that $i = \sum_{r=1}^{m} i_r 2^{r-1}$ and π is a permutation of $\{1, 2, \cdots, m\}$. Eqn. (2.60) generates $2^{h(m+1)} m!/2$ Golay sequences over $\mathbb{Z}_{2^h}$. This defines a 2^h-ary $(2^m, m+1)$ block code that can be viewed as a second order co-set of a Reed-Muller code [15]. By ignoring the coset terms in (2.60), $\mathbf{c}$ can be represented in the conventional block code format as

$$\mathbf{c} = \mathbf{d} \cdot G + \mathbf{b} \qquad (2.61)$$

where $G_{(m+1)\times 2^m}$ is the generator matrix, $\mathbf{d} = (d_0, d_1, \cdots, d_m)$, $\mathbf{b}$ represents the coset term, and arithmetic is mod q.

There are $m!/2$ possible coset terms in (2.60) and they can be used to transmit an additional $\log_2(m!/2)$ bits which will slightly increase the decoder complexity to retrieve the coset terms. In the next chapter, the problem of ML decoding of Golay sequences and related codes is discussed in detail.

2.7 Conclusion

This chapter focused on the review of the developments pertaining to OFDM. OFDM has now been standardized for local area networks (LAN). We reviewed

the recent standards and discussed the fundamentals of OFDM. Mathematical representations of OFDM signals as well as nonlinear communication channels were also discussed. We also presented statistical and analytical approximations for the distribution of PAPR of OFDM signals and lastly, we provided an overview of existing PAPR reduction techniques.

Chapter 3

Efficient Decoding of Golay Sequences

The use of Golay sequences is a promising solution to the problem of PAPR in OFDM systems. In this chapter, we focus on the optimum decoding of the Golay codes with reasonable complexity. First, we review the existing decoding techniques in the literature. Then, we introduce our proposed algorithm and evaluate its performance and complexity. The choice of initial parameters is discussed afterwards and an even lower complexity algorithm is proposed using improved lower bounds. Finally, we present simulation results to compare the complexity and BER performance of our proposed decoders to existing techniques.

3.1 Background

Efficient and optimal (*i.e.*, soft-decision ML) decoding of Golay sequences and RM codes is an important problem for OFDM systems. ML decoding requires computing the Euclidean distance or (equivalently) the correlation between the received vector and all valid codewords. These correlations can be efficiently

computed using the fast Hadamard transform (FHT); an FHT decoder for first-order RM codes is developed in [25]. While the FHT decoder efficiently computes the correlations, its complexity remains high. Another decoding approach is to reorder the received symbols according to a reliability measure; see [22] for a review of such techniques. Ordered statistics decoding (OSD) is an example of this approach that has been extended to Golay sequences in OFDM [48]. OSD is a low complexity decoding technique for codes with moderate or high rates. However, for codes with low rates, such as Golay sequence codes, this technique requires extensive computation. Finally, classical hard-decision RM decoding algorithms include majority logic and threshold decoding schemes. These decoders are simple and fast, but suboptimal. A class of sub-optimal soft decision decoding algorithms for RM codes using majority logic decoding has also been developed [55].

In this chapter, we propose a low-complexity decoding technique for Golay-sequence block codes[1]. ML decoding of an (n, k) linear binary code is an NP-hard problem with computational complexity $\mathcal{O}(2^{\min(k,n-k)})$ [86]. In complexity-theoretic terms, this means that no decoding algorithm is likely to be discovered that solves every instance of the decoding problem with a running time that grows only polynomially with the problem size. NP-hardness implies that a decoding algorithm may require exponentially growing time. But it is well-known that soft-decision ML decoding achieves a gain of 3 dB or more over sub-optimal hard-decision algorithms and this has resulted in strong research efforts to find near-MLD algorithms which have reasonable complexity(see [88] and references therein).

It is now known that an exponentially-hard problem can be solved in polynomial time for certain regions in the parameter space. As one realization of

[1]Note that the famous $(23, 12)$ Golay code is an entirely different code.

this situation, sphere decoding (SD) for lattice codes has caused much excitement in the research community because SD has polynomial (cubic) complexity in the high SNR region [2,14,16,28]. Using the key idea of sphere decoding, we develop an efficient ML decoder for Golay sequences used for peak-reduction in OFDM. The algorithm requires substantially fewer computational operations than existing ML algorithms and is even more efficient than the suboptimal algorithms mentioned above. This means that we can achieve ML performance without resorting to suboptimal strategies, at least in the high SNR region.

We also provide further improvements to the algorithm and consider both phase-shift keying and quadrature amplitude modulation. Measures of complexity are also developed. Simulation results are carried out for both AWGN and fading channels as well as for amplifier non-linearities. Finally, the application of the proposed decoder for efficient design of an OFDM-based differentially coherent receiver is investigated.

3.2 Existing Decoding Techniques

For comparison with the new decoding technique we propose in the next section, we now present a brief description of ML, OSD and majority logic decoding techniques for Golay sequences. Let the transmitted codeword be $\mathbf{c} = (c_0, c_1, \cdots, c_n)$ as defined in (2.61), and let the corresponding received signal be $\mathbf{r} = (r_0, r_1, \cdots, r_n)$.

1. **Maximum Likelihood Decoding** : Conditional probabilities Pr ($\mathbf{r}$ received|$\mathbf{c}$ sent) are computed for all valid codewords $\mathbf{c}$. The ML estimate is the codeword that results in maximum probability, *i.e.*, Pr ($\mathbf{r}$ received|$\hat{\mathbf{c}}_{ML}$ sent) $= \max_{\mathbf{c} \in C} P(\mathbf{r} \text{ received} | \mathbf{c} \text{ sent})$(see Eqn.(4.11)).

2. **Ordered Statistics Decoding** : OSD [22] requires calculation and

ranking of reliability metrics. For binary codes, the reliability metric is the amplitude of the received symbol. For non-binary cases, the reliability measure is computed as follows. Let $\hat{\mathbf{r}} = (\hat{r_0}, \hat{r_1}, \cdots, \hat{r_n})$ denote the hard-decision decoded symbol vector corresponding to $\mathbf{r}$. The reliability of the ith symbol is defined as [48]

$$\mathcal{L}_i \triangleq \ln \frac{\Pr[r_i|\hat{r}_i]}{\sum_{r_i \neq \hat{r}_i} \Pr[r_i|\hat{r}_i]}. \tag{3.1}$$

The OSD algorithm is then summarized as follows [48].

(a) **Initial processing(Order-0)** : Rank the received samples in decreasing order of reliability to yield $\acute{\mathbf{r}} = (\acute{r_0}, \acute{r_1}, \cdots, \acute{r_n})$, with the additional condition that the first $m+1$ columns of the generator matrix permuted in the same order as $\acute{\mathbf{r}}$ are independent. The permuted generator matrix G' can therefore be expressed in a systematic form.

(b) **Order-i re-processing**: For each phase $l, 1 \leq l \leq i$, generate all possible combinations of the l most reliable symbols, generate the corresponding codewords based on G', and find the correlation with $\acute{\mathbf{r}}$.

(c) **Final decision**: Choose the codeword with the maximum correlation among all generated candidates.

3. **Majority Logic Decoding** : The Sylvester-Hadamard matrix $\mathbf{H}_{2^m} = [H_{i,j}]$ of order 2^m is defined as

$$H_{i,j} = (-1)^{\sum_{k=1}^{m} i_k j_k} \qquad \text{for } i, j \in \mathbf{Z}_{2^m} \tag{3.2}$$

where $(i_1, i_2, \cdots, i_m)$ and $(j_1, j_2, \cdots, j_m)$ are the binary representations

of i and j, respectively. The fast Hadamard transform (FHT) of a vector $\mathbf{y} = (y_0, \cdots, y_{2^m-1})$ is defined as $\hat{\mathbf{y}} = \mathbf{y}H_{2^m}$. Majority logic decoding for $RM_{2^h}(1, m)$ codewords requires h FHT's and h encoding operations as outlined below [15].

(a) Set $k = 0$ and $r_0 = r$.

(b) Define the sequence $(y)_i = 2^{k-1} - \min\left((r_k)_i \mod 2^{k+1}, 2^{k+1} - (r_k)_i \mod 2^{k+1}\right)$ for $i = 0, 1, \cdots, 2^m - 1$ where $(\chi)_i$ represents the i-th bit in the binary representation of χ.

(c) Let $\hat{y}$ be the FHT of y. Also let $j \in \mathbb{Z}_{2^m}$ be the value for which $(\hat{y})_j$ is an element of $\hat{y}$ with the largest magnitude. Let w be 0 or 1 according to whether $(\hat{y})_j$ is positive or negative, and let $(w_1, w_2, \cdots, w_m)$ be the binary representation of j. Set $f_k = (\sum_{i=0}^{m} w_i x_i + w) \mod 2^{h-k}$.

(d) If $k = h-1$ then output the codeword $(2^{h-1}f_{h-1} + 2^{h-2}f_{h-2} + \cdots + f_0) \mod 2^h$. Else set $r_{k+1} = \left(r_k - 2^k f_k\right) \mod 2^h$, increment k, and go to step b).

3.3 Reduced Complexity ML Decoding

We now develop an efficient ML decoder for Golay sequences. The sphere decoding (SD) algorithm that has been developed for decoding lattice codes is based on a bounded distance search among the lattice points which fall inside a sphere of a predefined radius [16]. However, Golay sequences are not decodable with this algorithm because these sequences cannot be represented with a simple lattice description.[2] We adapt the key idea of sphere decoding to limit the search space only to the points in a multi dimensional sphere centered

[2] A lattice code is a set $\{\mathbf{x} \cdot G | \mathbf{x} \in D^k\}$ where G is a matrix and D is an integer set. The code (2.61) is not a lattice code because of the use of modulo-q addition.

around the received signal.

SD can alternatively be viewed as a tree decoder, which is also useful for understanding our new algorithm. For instance, an (n, k) block code can be represented by a tree of $(k+1)$ levels where all nodes in the l-th level $(1 \leq l \leq k)$ correspond to lattice points of dimension l. Starting with $l = 1$, the lattice points of dimension l are tested to see if they are inside a sphere of radius μ. The lattice points (or nodes) outside the sphere are pruned (*i.e.*, no descendent nodes are generated) and removed from further processing. The minimum distance node among the nodes remaining in the k-th level will be the ML-estimate. If no codeword is found, μ can be increased and the search can be repeated until a solution is found[3]. We adapt this approach to our problem at hand.

Given the transmitted OFDM signal (2.5), and assuming the channel response is shorter than the cyclic prefix, the received samples after DFT demodulation can be expressed as

$$r_i = \rho_i \xi^{c_i} + w_i, \qquad i = 0, \cdots, n-1, \tag{3.3}$$

where ρ_i are the fading coefficients corresponding to each sub-channel and where $w_i \sim \mathcal{CN}(0, \sigma^2)$ is a complex AWGN term with zero mean and variance σ^2. The vector $\rho = (\rho_0, \rho_1, \cdots, \rho_{n-1})$ is the channel state information (CSI) which can be obtained, for example, by use of pilot symbols. Note that for AWGN channels, $\rho_i = 1$ and for a slow fading channel, $\rho_i = H(2\pi i/n)$ where $H(\omega)$ is the Fourier transform of the channel impulse response.

[3]Note that in some implementations of SD, if no codeword is found for the initial choice of μ a decoding failure is declared. This will result in a suboptimal algorithm whose performance approaches that of ML only in the high SNR region. Since we recommend increasing μ until a solution is found, our algorithm is ML for all SNR values. Simulation results reported later in this thesis confirm this result. For low SNR values the complexity of our algorithm increases rapidly.

The ML solution $\hat{\mathbf{c}}_{ML}$ is found by computing the distance metric for all possible codewords:

$$\hat{\mathbf{c}}_{ML} = \arg \min_{\mathbf{a} \in GS(n)} \underbrace{\sum_{i=0}^{n-1} |r_i - \rho_i \zeta^{a_i}|^2}_{\Lambda(\mathbf{a})}. \tag{3.4}$$

A brute force calculation of (4.11) for a (n, k) block code is exponential in k because the metric has to be computed q^k times. Throughout the thesis, exhaustive computation of (4.11) for all codewords is referred to as (brute-force) MLD.

3.3.1 Proposed Decoding Algorithm (Algorithm 1)

Note that there are q^{m+1} codewords. With SD, instead of exhaustively computing $\Lambda(\mathbf{a})$ for each codeword, we propose iteratively locating codewords which satisfy $\Lambda(\mathbf{a}) < \mu^2$ for some real positive μ. This general idea of our algorithm can be summarized as follows:

1. Initialize μ
2. Generate the feasible set FS= $\{\mathbf{a} | \mathbf{a} \in GS(n)$ and $\Lambda(\mathbf{a}) < \mu^2\}$
3. If FS is non-empty, pick the member $\mathbf{a}$ of FS with the smallest metric $\Lambda(\mathbf{a})$. This will be the ML solution $\hat{\mathbf{c}}_{ML}$. If FS is empty, increase μ and go to step 2.

Step 2 must be realized as efficiently as possible. Since we are decoding $(2^m, m+1)$ block codes, we represent $\Lambda(\mathbf{a})$ as a sum of $m+1$ partial metrics as follows. From (2.61), $\Lambda(\mathbf{a})$ can be written as $\Lambda(\mathbf{b} \cdot G)$, and since G is deterministic, $\Lambda(\mathbf{a})$ can be replaced by $\Lambda(\mathbf{b})$. The metric can then be written

in terms of the sub-metrics $\Lambda_i(\mathbf{b})$ iteratively as

$$\Lambda_i(b_0,\cdots,b_{i-1}) = \Lambda_{i-1}(b_0,\cdots,b_{i-2}) + \sum_{k\in S_i} \left|r_k - \rho_k \xi^{\mathbf{b}\cdot\mathbf{g}_k}\right|^2 \ , \ i = 2,3,\cdots,m+1 \tag{3.5}$$

with the initial condition $\Lambda_1(b_0) = \left|r_0 - \xi^{b_0}\right|^2$, where $G = [\mathbf{g}_1, \mathbf{g}_2, \cdots, \mathbf{g}_{2^m}]$, $\mathbf{g}_k = [g_{k,1}, g_{k,2}, \cdots, g_{k,m+1}]^T$, $g_{k,r} \in \mathbb{Z}_q$, and where S_i is the set of the indices of columns in G which contain non-zero elements in the i-th row and no non-zero elements in the l-th row for all $i > l$. That is

$$S_i = \{k | g_{k,i} \neq 0, g_{k,l} = 0, \text{ for all } l > i, k = 1,\cdots,2^m\} \tag{3.6}$$

Note that $\Lambda(\mathbf{b}) \geq \Lambda_i(b_0,\cdots,b_{i-1})$ for all $i = 1,\cdots,m+1$, therefore the decoding procedure is translated into computation of the sub-metrics that satisfy the following inequality

$$\Lambda_i(b_0,\cdots,b_{i-1}) < \mu^2. \tag{3.7}$$

Note also that $(b_0,\cdots,b_{i-1})$ can be interpreted as a node in the i-th level $(1 \leq i \leq m)$ in the tree. There are q^i such nodes in total. Those for which (3.7) is not satisfied can be pruned immediately while retaining the optimality of the search.

This decoding algorithm is described in detail in the following pseudo-code entitled Algorithm 1. The algorithm constructs a tree with q branches from each node representing the q constellation points. To decode a received vector, all nodes which violate (3.7) are pruned.

We provide a simple example to compare exhaustive ML decoding with decoding using Algorithm 1. Fig.3.1a and 3.1b show the trees for ML and Algorithm 1 for an $(8,4)$ binary PSK-OFDM code. Codewords are generated

according to (2.60); there are 16 codewords in total. Exhaustive ML computes the distance metric (4.11) for all nodes in level 4 (numbered 16 to 31). This is equivalent to traversing the entire tree in Fig.3.1a. For clarity, the sub-metric of each node is not shown.

Let $\mu = 2.64$ be the initial sphere radius for our new algorithm. This is selected according to (3.10) as discussed in the next subsection. When nodes 4 and 5 are generated, they already violate (3.7) and hence are pruned. That is, the distance between the received vector and any codeword with $b_0 = 0$ is not computed. Similarly, nodes (6) and (14) are pruned, eliminating codewords with $b_1 = 0$ and $b_2 = 0$ from further consideration. Algorithm 1 results in only two nodes in level 4, and clearly node (31) provides the minimum distance solution. Note that exhaustive ML requires processing 31 nodes, whereas Algorithm 1 processes only 11 nodes. For high SNRs and for longer codes, complexity savings such as these can be extremely large.

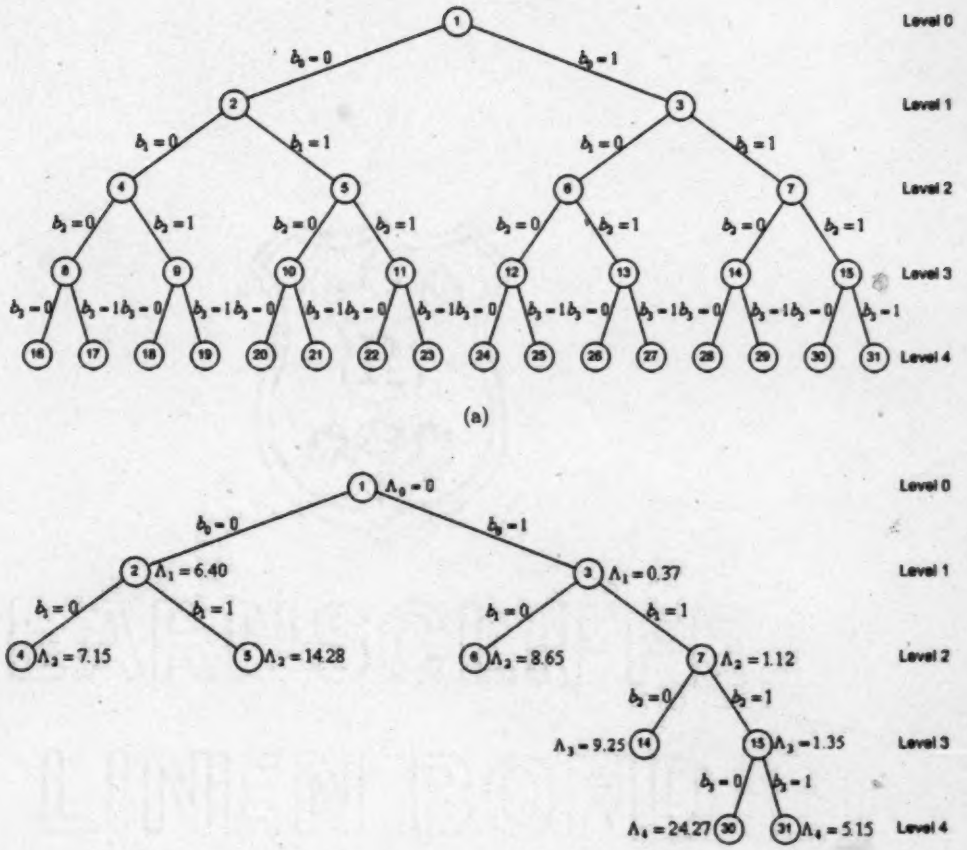

Figure 3.1: (a) Illustration of MLD for the RM(8, 4) BPSK code and $SNR_b = 7$ dB. (b) Illustration of Algorithm 1 for the RM(8, 4) BPSK code and $SNR_b = 7$ dB.

Algorithm 1: GOLAY DECODER($\mathbf{r}, G, \mu$)

1) Initialize $\mathbf{r}, \mu, \Lambda_1(b_0) = \left|r_0 - \rho_0 \xi^{b_0}\right|^2$

2) **if** $\Lambda_1(b_0) \leq \mu^2$

then { Save the value of b_0 ; $\mathrm{i} = 2$

3) $S_\mathrm{i} = \{k | g_{k,\mathrm{i}} \neq 0, g_{k,l} = 0, \text{ for all } l > \mathrm{i}, k = 1, \cdots, 2^m\}$

while $\mathrm{i} \leq m$

do { **for each** choice of b_i

do { **if** $\sum_{k \in S_\mathrm{i}} \left|r_k - \rho_k \xi^{\mathbf{b} \cdot \mathbf{g}_k}\right|^2 + \Lambda_{\mathrm{i}-1}(b_0, \cdots, b_{\mathrm{i}-2}) < \mu^2$

then { Save the value of b_i ; $\mathrm{i} = \mathrm{i} + 1$

else { Delete the current sequence $\mathbf{b}$

4) Among the set of resulting $\mathbf{b}$, choose the one with lowest Euclidean distance to $\mathbf{r}$. If no result for $\mathbf{b}$ is found, increase μ and go to step 1)

3.3.2 Initial Choice of The Radius of Sphere (μ)

We choose μ so that with high probability, at least one codeword is inside $\Lambda(\mathbf{a}) < \mu^2$. The distance metric corresponding to the true transmitted codeword is

$$\Lambda(\mathbf{c}) = \sum_{i=0}^{2^m - 1} |w_i|^2 \qquad (3.8)$$

where $w_i \sim \mathcal{CN}(0, \sigma^2)$. The distribution of Λ is consequently *chi-square* with 2^{m+1} degrees of freedom and its cumulative distribution function (CDF) is [58]

$$F_\Lambda(\lambda) = \int_0^\lambda \frac{1}{\sigma^{2^{m+1}}\Gamma(2^m)} y^{2^m-1} e^{-y/\sigma^2} dy. \tag{3.9}$$

We choose μ to be α percentile of its CDF. This gives

$$\mu = F_\Lambda^{-1}(\alpha) \tag{3.10}$$

and we set $\alpha = 0.99$ in our simulations. If a solution does not exist within this sphere, we double μ and repeat the algorithm until a solution is found.

3.3.3 Using Improved Lower Bounds in Algorithm 1

Although Algorithm 1 offers a significant reduction in complexity compared to exhaustive MLD, complexity can be further reduced. The key idea is to strengthen (3.7) by improving the sub-metrics $\Lambda_i(b_0, \cdots, b_{i-1})$. In order to improve $\Lambda_i(b_0, \cdots, b_{i-1})$, we consider $\Lambda(\mathbf{b})$ as

$$\Lambda(\mathbf{b}) = \Lambda_i(b_0, \cdots, b_{i-1}) + \sum_{k \in J_i} \left| r_k - \rho_k \xi^{\mathbf{b} \cdot \mathbf{g}_k} \right|^2. \tag{3.11}$$

where J_i are the sets of indices of subcarriers whose modulation symbols are determined by $b_i, \cdots, b_m$. The sum in (3.11) can be bounded as

$$\sum_{k\in J_c}\left|r_k-\rho_k\xi^{\mathbf{b}\cdot\mathbf{g}_k}\right|^2=\sum_{k\in J_c}\left(|r_k|^2+|\rho_k|^2-2\mathrm{Re}\left(r_k\cdot\rho_k^*\xi^{-\mathbf{b}\cdot\mathbf{g}_k}\right)\right)$$
$$=\sum_{k\in J_c}\left(|r_k|^2+|\rho_k|^2-2\left|r_k\rho_k\right|\cos\left(\angle r_k-\angle\rho_k\xi^{\mathbf{b}\cdot\mathbf{g}_k}\right)\right)$$
$$\geq\sum_{k\in J_c}\left(|r_k|-|\rho_k|\right)^2. \qquad (3.12)$$

Assuming that the channel coefficients ρ_k are known, the sub-metrics $\Lambda_i(b_0,\cdots,b_{i-1})$ can be increased by the upper bound in (3.12). Let us define the improved sub-metric Λ' as

$$\Lambda'(b_0,\cdots,b_{i-1})=\Lambda_i(b_0,\cdots,b_{i-1})+\sum_{k\in J_c}\left(|r_k|-|\rho_k|\right)^2. \qquad (3.13)$$

Incorporating Λ' from (3.13) in Algorithm 1 results in an improved algorithm which we refer to as Algorithm 2. Note that in the low SNR regime, both algorithms have the same performance (Fig. 3.8). It is interesting to note that $(|r_k|-|\rho_k|)$ is a measure of the additive noise level in a sample.

3.4 Numerical results

3.4.1 Performance of The Proposed Decoding Algorithms in AWGN and Fading Channels

We consider the performance of our algorithms in terms of decoded bit error rate (BER) and decoder complexity. Fig. 3.2 and Fig. 3.3 compare the BER performance of MLD, OSD, majority logic decoding (MALD) and Algorithm 1 for the RM$(16,5)$ code with 8-PSK modulation and the RM$(32,6)$ code with QPSK modulation in an AWGN channel. MLD is implemented by exhaustive

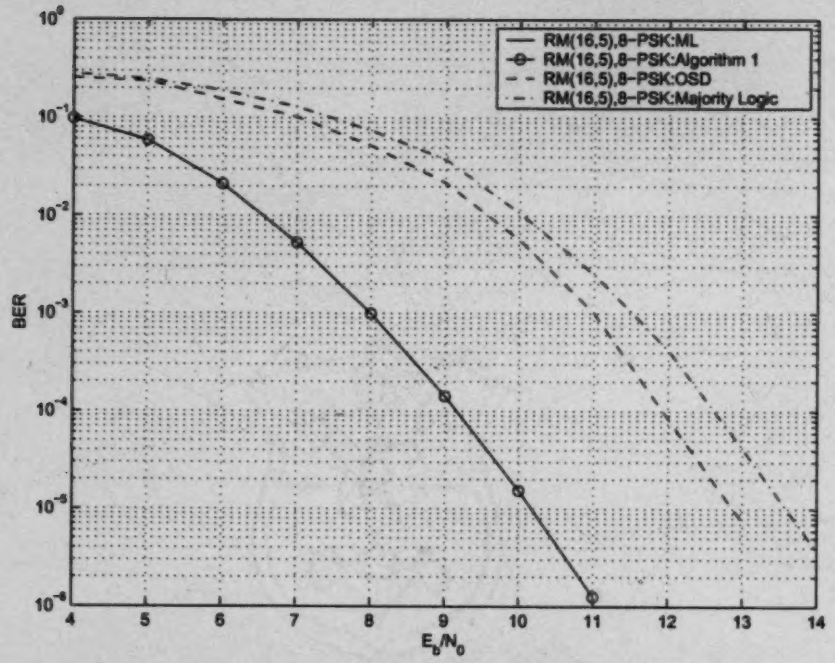

Figure 3.2: BER comparison for MLD, Algorithm 1, OSD and majority logic decoding for RM(16,5) in an AWGN channel using 8-PSK modulation. Note that the MLD and Algorithm 1 curves coincide exactly.

search (4.11). The BER curves of Algorithm 1 and MLD coincide as expected. Algorithm 1 outperforms both OSD and MALD with approximately 3 dB SNR improvement for RM(16, 5) and 4 dB for RM(32, 6).

We also considered the BER performance of the new decoder for a fading channel and perfect channel estimation. In this simulation we used the typical channel profiles of indoor office areas with moderate delay spread ($\tau_{rms} = 35ns$) [49]. Fig. 3.4 and 3.5 demonstrate that Algorithm 1 performs better than both OSD and majority logic decoding under these conditions. Our algorithm yields approximately 7 dB improvement for the RM(16, 5) code and at least 5 dB improvement for the RM(32, 6) code.

The computational complexity of our algorithms depend on the number

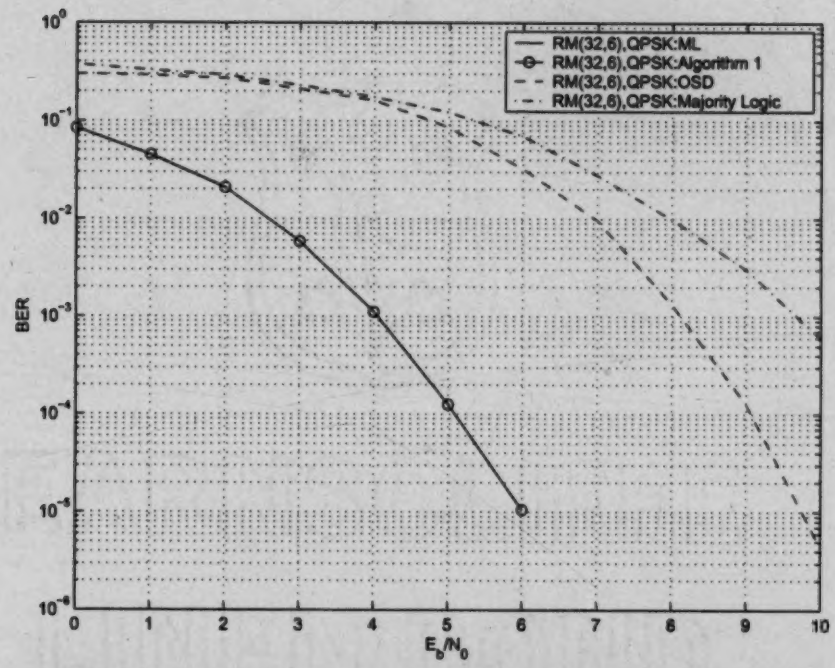

Figure 3.3: BER comparison for MLD, Algorithm 1, OSD and majority logic decoding for RM(32,6) in an AWGN channel using QPSK modulation. Note that the MLD and Algorithm 1 curves coincide exactly.

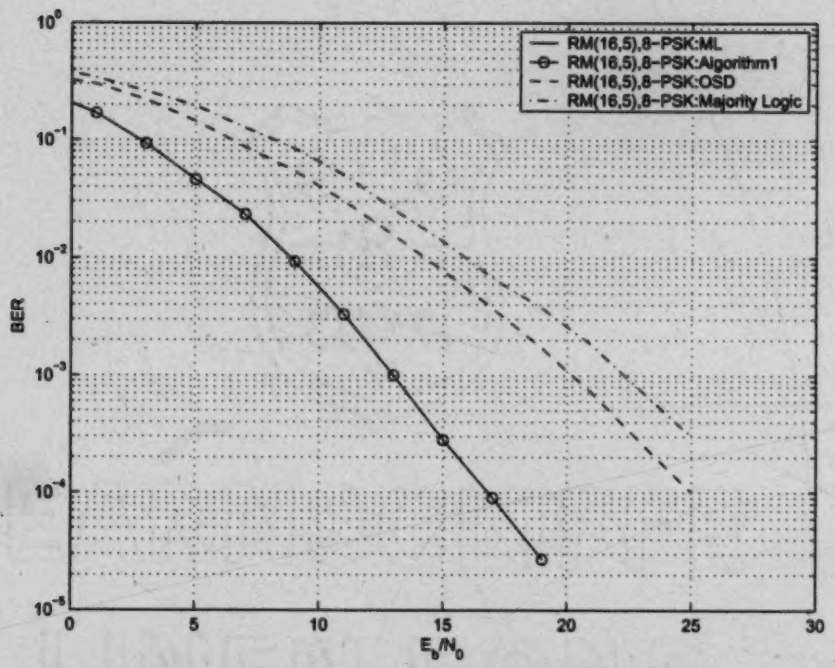

Figure 3.4: BER comparison for MLD, Algorithm 1, OSD and majority logic decoding for RM(16,5) in a fading channel using 8-PSK modulation. Note that the MLD and Algorithm 1 curves coincide exactly.

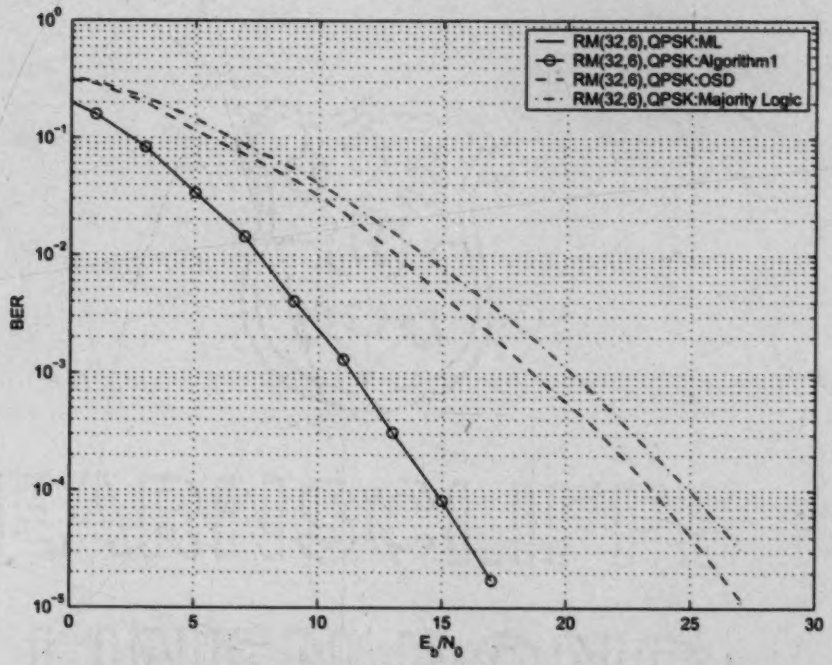

Figure 3.5: BER comparison for MLD, Algorithm 1, OSD and majority logic decoding for RM(32,6) in a fading channel using QPSK modulation. Note that the MLD and Algorithm 1 curves coincide exactly.

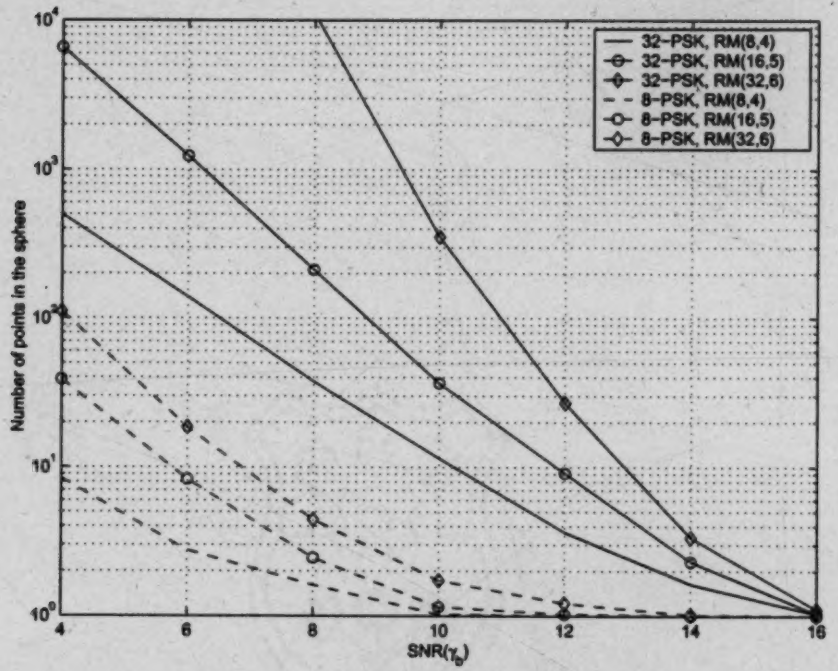

Figure 3.6: Number of codewords in the constructed spheres for first order Reed-Muller codes with 8-PSK and 32-PSK modulation.

of nodes which are visited. Fig. 3.6 depicts the total number of codewords found in the constructed sphere versus the signal to noise ratio (SNR) when the $(8,4)$, $(16,5)$ and $(32,6)$ first order Reed-Muller codes are used. As shown in this figure, the complexity of Algorithm 1 decreases with increasing SNR such that on average, less than 10 codewords in the sphere are examined when $SNR > 6.8$ dB and the 8-PSK constellation is used. Also, $SNR > 13$ dB ensures that the algorithm considers nearly 10 codewords in most cases when 32-PSK is used with RM$(8,4)$. By comparison, ML requires more than 2^{20} computations, since the complexity of MLD grows exponentially with code length regardless of the SNR whereas in our technique the complexity reduces with increasing SNR.

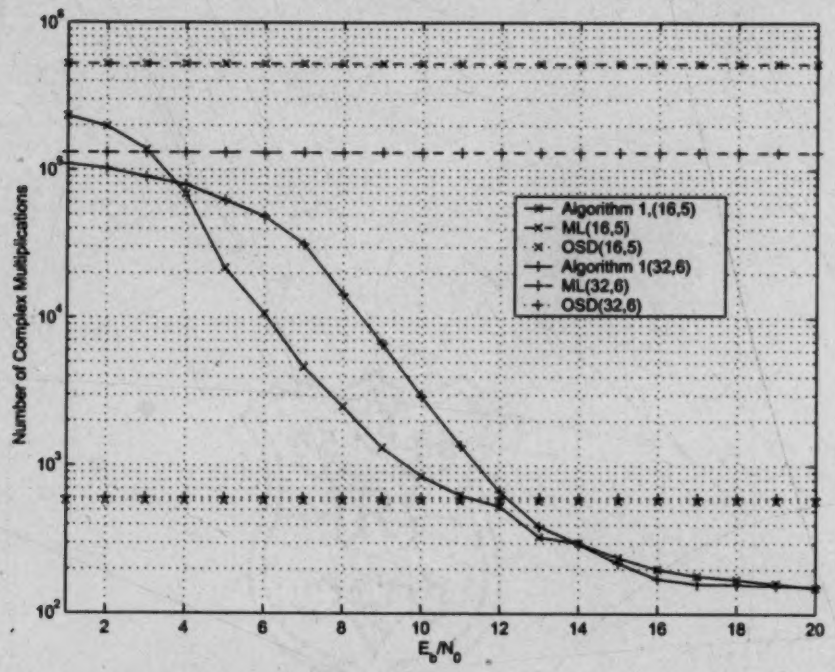

Figure 3.7: Comparison of the number of required complex multiplications in MLD, Algorithm 1 and OSD.

As another measure of computational complexity, in Fig. 3.7 we consider the number of complex multiplications required for MLD, OSD and Algorithm 1. For MLD, the number of complex multiplications is independent of SNR. In the low SNR regime, the complexity of Algorithm 1 approaches that of MLD but at higher SNR, our algorithm offers the same BER performance with significantly lower complexity. For instance, at an SNR of 10 dB, MLD of the RM$(16, 5)$ code requires 10^5 multiplications whereas Algorithm 1 requires about 3×10^3 multiplications. For the RM$(32, 6)$ code, MLD and Algorithm 1 require 5×10^5 and 8×10^2 multiplications, respectively. Moreover, the results show that in both cases, the complexity of our algorithm is less than that of OSD when SNR$>$ 12 dB.

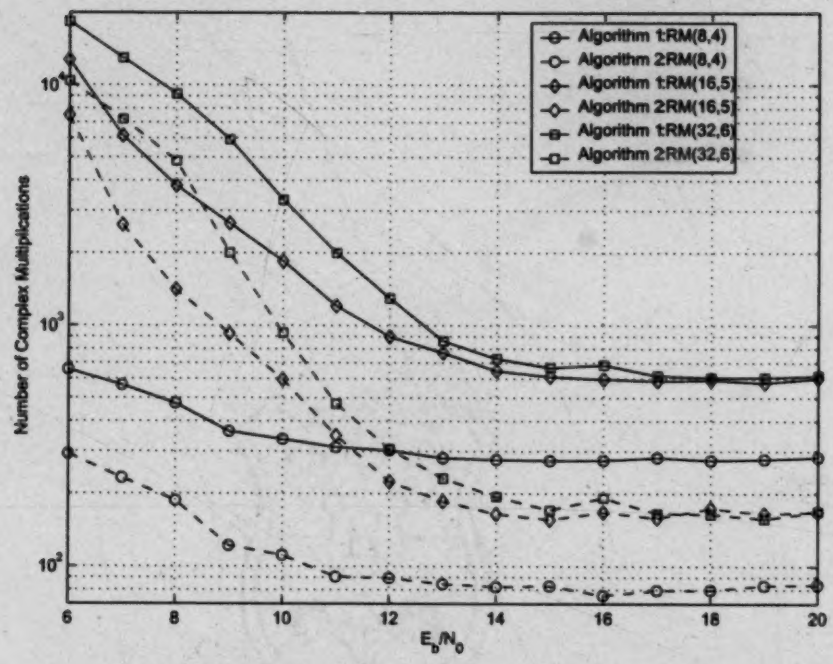

Figure 3.8: Comparison of the number of required complex multiplications in Algorithm 1 and Algorithm 2.

To quantify the complexity reduction available with Algorithm 2, we consider the average number of complex multiplications necessary to decode a received vector $\mathbf{r}$. Our averages were taken over $10,000$ decoded codewords for each value of SNR. Fig. 3.8 compares the number of multiplications for Algorithm 1 and Algorithm 2. At high SNR, Algorithm 2 requires approximately one-third the multiplications. For instance, for the RM$(16,5)$ code, 600 complex multiplications are required to decode the received signal with Algorithm 1 whereas, on average, only 180 multiplications are required for Algorithm 2.

3.5 Conclusion

In this chapter, an overview of the existing decoding techniques for Golay-based codes was provided. It was shown that in all these existing decoding techniques, complexity reduction is at the cost of decoding performance. We proposed a novel optimum decoding algorithm for Reed-Muller codes based on the idea of sphere decoding. We showed that although the complexity of our algorithm approaches that of ML decoding in the low SNR regions, in the high SNR region, it achieves significant complexity savings. Following that, a statistical approach to the choice of initial parameters of the proposed decoder was developed and then, using the improved lower bounds, an algorithm with even lower complexity was proposed. Finally, simulation results were provided to evaluate the BER performance and complexity saving capability of the proposed decoders.

Chapter 4

Extension of The Proposed Algorithm and Complexity Analysis

In the previous chapter, we introduced a novel optimum decoder for Golay-based sequences. This chapter extends the application of that decoding algorithm to QAM, as well as to differential MDPSK transceivers. We present simulation results to compare our decoding algorithm with existing decoders in terms of BER performance as well as complexity. Lastly, we develop an analytical approximation for the complexity of the decoder proposed in the previous chapter.

4.1 Decoding Low PAPR QAM Sequences Based on Golay Sequences

The low PAPR sequences introduced in (2.60) are used with PSK, a constant modulus signalling constellation. In practice, OFDM is commonly used

with M-ary quadrature amplitude modulation (QAM). Golay sequences can be extended to construct QAM sequences with bounded PAPR. Let us define $\mathbf{c}^K = (c_0^K, \cdots, c_{n-1}^K), K = 0, \cdots, N-1$ to be N Golay sequences in $\mathbf{Z}_4$ (*i.e.* $c_i^K \in \mathbf{Z}_4$). Also let us assume $\mathbf{c}^K = \mathbf{b}^K \cdot G$, according to (2.61) where $\mathbf{b}^K = (b_0^K, \cdots, b_{k-1}^K)$. A 4^N-QAM OFDM signal can be formed according to [4]

$$S_{c^0,c^1,\cdots,c^{N-1}}(t) = \sum_{K=0}^{N-1}\sum_{i=0}^{n-1}(2^i)(\frac{\sqrt{2}}{2})j^{c_i^K}\exp\left(2\pi j\left(f_0 + Kf_s\right)t + \frac{\pi j}{4}\right) \quad (4.1)$$

It can be shown that the PAPR of (4.1) is limited to $\frac{6\left(2^N-1\right)^2}{2^{2N}-1}$ [4]. For the practical case of $N = 2$, the PAPR of the 16-QAM signal is bounded by 3.6. Again if MLD is implemented via exhaustive search, decoding complexity becomes exponential in the worst case. However, a similar approach to that we propose for PSK modulation can be followed for reduced complexity ML decoding of QAM Golay sequences. The ML solution for QAM codewords is

$$\hat{\mathbf{c}}_{ML}^0, \cdots, \hat{\mathbf{c}}_{ML}^{N-1} = \arg \min_{(\mathbf{a}^0,\cdots,\mathbf{a}^{N-1})\in GS^{N-1}(n)} \underbrace{\sum_{i=0}^{n-1}\left|r_i - \sum_{K=0}^{N-1}(2^i)(\frac{\sqrt{2}}{2})j^{a_i^K}\right|^2}_{\Lambda(\mathbf{a}^0,\cdots,\mathbf{a}^{N-1})}. \quad (4.2)$$

The metric (4.2) can be written in terms of the sub-metrics $\Lambda_i\left(\mathbf{a}^0, \cdots, \mathbf{a}^{N-1}\right)$ as

$$\Lambda_i\left(\mathbf{a}^0, \cdots, \mathbf{a}^{N-1}\right) = \Lambda_{i-1}\left(\mathbf{a}^0, \cdots, \mathbf{a}^{N-1}\right) + \sum_{k\in S_i}\left|r_k - \sum_{K=0}^{N-1}(2^k)(\frac{\sqrt{2}}{2})j^{a_k^K}\right|^2 \quad (4.3)$$

where S_i is defined in Section 3.3.1. Eqn. (4.3) motivates the construction of a tree similar to that previously constructed for PSK codewords, and Algorithm 1 introduced in Section 3.3.1 can be modified with respect to (4.3) to efficiently decode the QAM codewords.

4.2 Performance of 16-QAM OFDM In Nonlinear Channels

OFDM signals with QAM modulation typically have a PAPR greater than 10 [45] and hence force the high-power amplifier (HPA) to work in saturation. This results in signal compression, out-of-band radiation and performance degradation. The QAM OFDM signals described by (4.1) result in less distortion in nonlinear channels than uncoded QAM-OFDM because of their low PAPR. Fig. 4.1 compares the BER performance of a coded 16-QAM OFDM signal with that of uncoded OFDM. The RM$(8,4)$ code is used to encode the data, and a Solid-State Power Amplifier (SSPA) is employed to simulate the HPA nonlinearity. The transfer function of the SSPA is given by (2.36). A practical amplifier is well approximated by choosing $p = 3$ [79]. We set A such that OFDM signals with PAPR of less than 4 (6 dB) pass through the linear region of the HPA. Fig. 4.1 shows that the nonlinearity of the amplifier severely degrades the performance of uncoded OFDM whereas it has no impact on that of coded OFDM due to its limited PAPR[1]. The BER performance of Algorithm 1 for QAM-OFDM signals is identical to that of ML, as expected.

4.3 Application of The Proposed Decoder in Differential M-ary DPSK-OFDM

In some applications, coherent detection cannot be used due to the complexity of the receiver. For instance, coherent detection requires that the frequency of the local oscillator in the receiver should be precisely equal to that of the

[1] As indicated in Section 4.1, the PAPR of a 16-QAM coded OFDM is 3.6

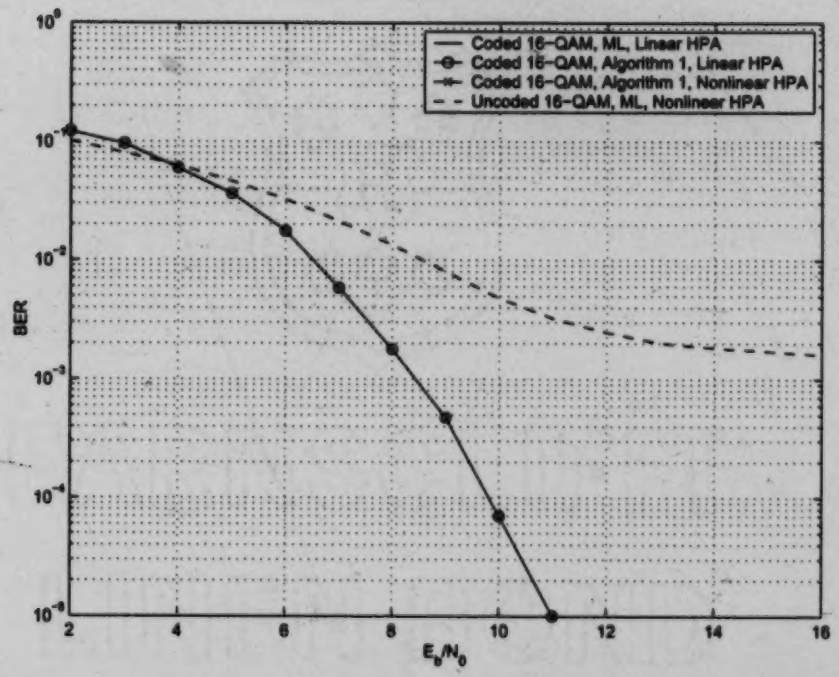
Coded 16−QAM, ML, Linear HPA
Coded 16−QAM, Algorithm 1, Linear HPA
Coded 16−QAM, Algorithm 1, Nonlinear HPA
Uncoded 16−QAM, ML, Nonlinear HPA
BER
E_b/N_0

Figure 4.1: BER performance of RM(8, 4) coded and uncoded QAM-OFDM with nonlinear amplifiers.

carrier frequency. However, extremely accurate oscillators are expensive. Alternatively, one can use differential modulation in the transmitter [58]. In differential modulator, the difference between adjacent data symbols is coded and transmitted across the channel. In the receiver, differential detection is used to detect the data [58].

Recently, a differential transceiver with low PAPR for frequency fading channels has been proposed in [49] and a suboptimal decoder has been proposed based on the extension of ordered statistics decoding (OSD) [22]. It was discussed in the previous sections that in codes with low rates such as Golay-based codes, OSD requires extensive computation while the BER performance might be far from ML. In this chapter, we apply our proposed decoding technique to the differential OFDM receiver and we compare the performance of the new transceiver with the results of [49].

In order to be consistent with the notation of [49], we rewrite (2.60) as

$$x_i = \sum_{k=1}^{m} u_k i_k + u_0 + \underbrace{2^{h-1} \sum_{k=1}^{m-1} i_{\pi(k)} i_{\pi(k+1)}}_{\text{coset term}}, \qquad i = 0, 1, \cdots, n-1, \tag{4.4}$$

where $[i_1, i_2, \cdots, i_m]$ and π are defined as in (2.60) and where $u_k \in \mathbb{Z}_{2^h}, k = 0, 1, \cdots, m$ are the source symbols. The resulting codeword $\mathbf{x} = [x_0, \cdots, x_{n-1}]$ can be represented in the conventional block code format using (2.61) as

$$\mathbf{x} = \mathbf{u} \cdot G + \mathbf{b}. \tag{4.5}$$

4.3.1 Differential Detection

Let $\mathbf{x}_0$ be the initial codeword in the differential decoder proposed in [49] such that $\mathbf{x}_0 = \mathbf{u}_0 \cdot G + \mathbf{b}$. For $l \geq 1$, the l-th symbol can be written as

$$\begin{aligned} \mathbf{x}_l &= (\mathbf{u}_l + \mathbf{u}_{l-1}) \cdot G + \mathbf{b} \\ &= \mathbf{x}_{l-1} + \mathbf{u}_l \cdot G \end{aligned} \tag{4.6}$$

and therefore,

$$\mathbf{d}_l = \mathbf{u}_l \cdot G \tag{4.7}$$

where $\mathbf{d}_l = \mathbf{x}_l - \mathbf{x}_{l-1}$ is the difference between the two successively transmitted codewords. Let $X_{l,m}$ be the complex-valued data symbol of the m-th subcarrier of the l-th OFDM symbol. The received signal can be expressed as

$$R_{l,m} = H_{l,m} \cdot X_{l,m} + N_{l,m} \tag{4.8}$$

where $H_{l,m}$ is the channel state information and where $N_{l,m}$ is a complex AWGN term. Given the differential transceiver described in [49], the output of the differential detector is

$$Y_{l,m} = R_{l,m} \cdot R^*_{l,m} \tag{4.9}$$

Assuming the channel is stationary over at least two successive symbols, we obtain

$$\begin{aligned} Y_{l,m} &= |H_{l,m}|^2 \, X_{l,m} \cdot X^*_{l,m} + \text{Noise Terms} \\ &= |H_{l,m}|^2 \, D_{l,m} + \text{Noise Terms} \end{aligned} \tag{4.10}$$

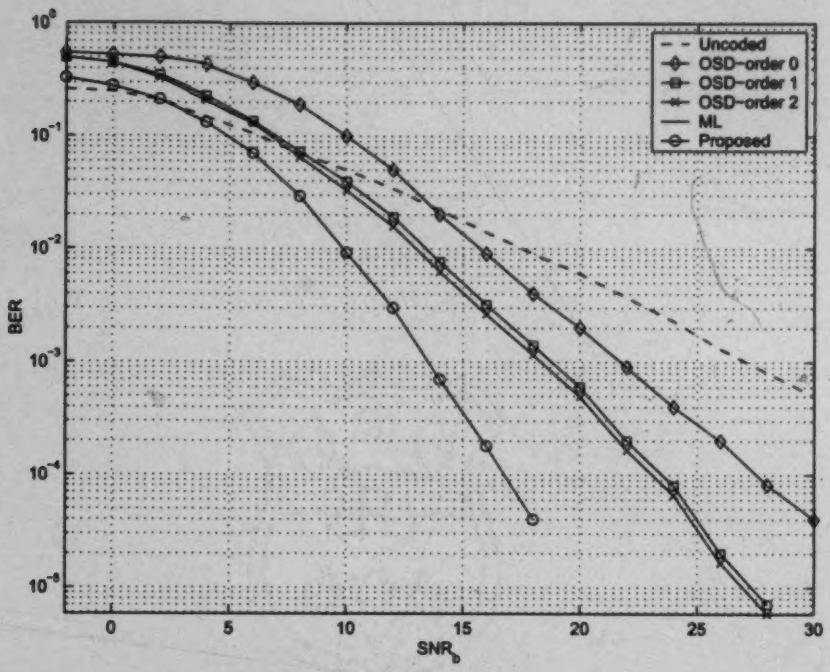

Figure 4.2: BER comparison for ML, Proposed Algorithm and OSD for RM(16,5) in a fading channel with 8-DPSK

where $D_{l,m} = \xi^{d_{l,m}}$.

Without loss of generality, we drop the frame index l for the rest of analysis. The ML solution $\mathbf{d}_{ML}$ is found by computing the following distance metric for all possible codewords:

$$\hat{\mathbf{d}}_{ML} = \arg \min_{\mathbf{d} \in GS(n)} \underbrace{\sum_{i=0}^{n-1} \left| y_i - \xi^{d_i} \right|^2}_{\Lambda(\mathbf{d})}. \tag{4.11}$$

A brute force calculation of (4.11) for a (n, k) block code is exponential in k as the metric has to be computed q^k times. In the proposed decoder, instead of exhaustively computing $\Lambda(\mathbf{d})$, valid codewords satisfying the constraint $\Lambda(\mathbf{d}) < \mu^2$ are iteratively found for some real positive μ as discussed in the

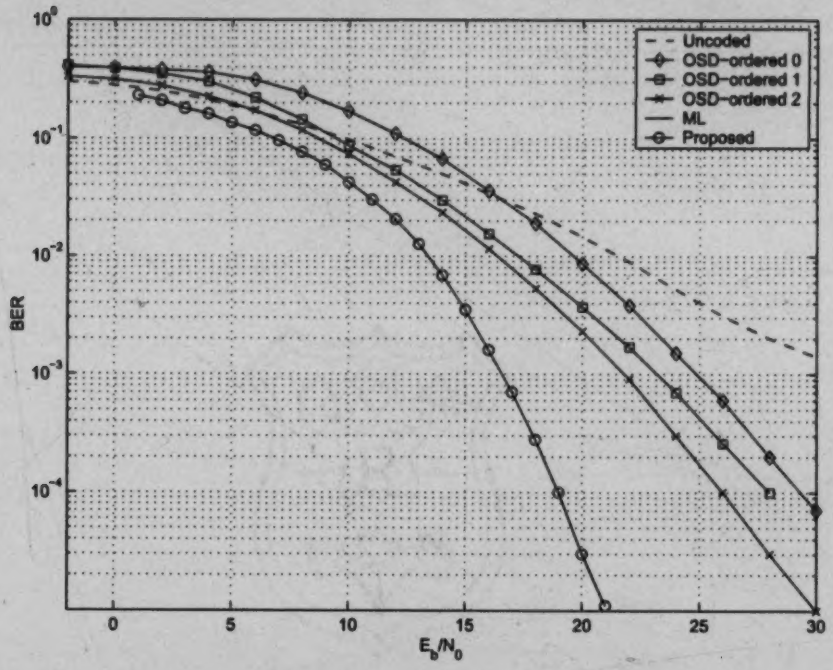

Figure 4.3: BER comparison for ML, Proposed Algorithm and OSD for RM(16,5) in a fading channel with QDPSK

previous chapter.

4.3.2 Performance Evaluation of the New MDPSK Receiver

Fig. 4.2 and Fig. 4.3 compare the BER performance of an MDPSK receiver employing ML, OSD and the proposed algorithm for RM$(16, 5)$ when 8-PSK and QPSK modulations are used in the frequency selective fading channel (channel A) described in [49]. The BER of the proposed algorithm coincides with that of ML. For a BER of 10^{-4}, the proposed algorithm outperforms OSD by 7 dB when QPSK is used and by 6 dB when 8-PSK is used. Fig. 4.4 compares the decoding time for ML, OSD and the proposed algorithm.

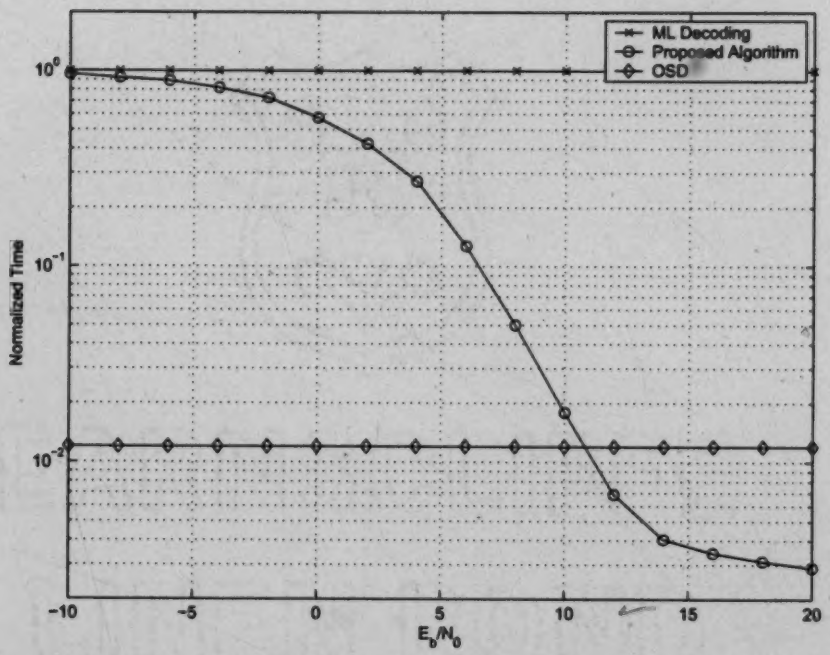

Figure 4.4: Decoding time comparison for ML, Proposed Algorithm and OSD for RM(16,5).

The time is normalized with respect to ML. The proposed algorithm requires less decoding time than ML. Moreover, in the high SNR region, the decoding time for the proposed algorithm is substantially less than that of both ML and OSD.

4.4 Complexity Analysis of The Proposed Decoding Technique

In Section 3.3.1, a low-complexity optimum decoder was proposed to decode the Golay-based codes. In this section, we analyze the complexity of the proposed algorithm. The worst case complexity (*i.e.* in the low SNR region) of our algorithm is exponential with codeword length. Similar to the analysis of SD, precise analysis of the complexity of this algorithm is difficult. A detailed analysis of the average complexity of SD can be found in [28]. As a complexity measure, we propose the average number of nodes visited by the algorithm. Note that the number of operations depends on the level of a node. This implies that more precise analysis would consider the average number of nodes at each level [28].

Consider the received signal r_i with channel gain $\rho_i = 1$ and noise $w_i \sim \mathcal{CN}(0, \sigma^2)$. MLD involves computation of the following metric for all valid codewords:

$$\Lambda(\mathbf{a}) = \sum_{i=0}^{n-1} |r_i - \xi^{a_i}|^2 = \sum_{i=0}^{n-1} |\rho_i (\xi^{c_i} - \xi^{a_i}) + w_i|^2 \qquad (4.12)$$

Let us define the random variables $X_{\mathbf{a}}$ as

$$X_{\mathbf{a}} = \begin{cases} 1 \text{ if } \Lambda(\mathbf{a}) < \mu^2 \\ 0 \text{ otherwise.} \end{cases} \tag{4.13}$$

and let T denote the number of codewords inside the sphere where $T = \sum_{\mathbf{a} \in GS(n)} X_{\mathbf{a}}$. Then

$$E(T) = \sum_{\mathbf{a} \in GS(n)} E(X_{\mathbf{a}}) = \sum_{\mathbf{a} \in GS(n)} \Pr\left[\Lambda(\mathbf{a}) < \mu^2\right].$$

The metric $\Lambda(\mathbf{a})$ in (4.12) is a noncentral Chi-square sum. From [58, (2.1-124)] we have

$$\Pr\left[\Lambda(\mathbf{a}) < \mu^2\right] = 1 - \mathcal{Q}_n\left(\frac{1}{\sigma}\sqrt{\sum_{i=0}^{n-1} |\xi^{c_i} - \xi^{a_i}|^2}, \frac{\mu}{\sigma}\right) \tag{4.14}$$

where the generalized Marcum $\mathcal{Q}_n$ function is defined in [58, (2.1-122)]. Therefore, for Golay-coded OFDM over an AWGN channel, the expected number of nodes processed by the proposed algorithm is

$$E(T) = \sum_{\mathbf{a} \in GS(n)} 1 - \mathcal{Q}_n\left(\frac{1}{\sigma}\sqrt{\sum_{i=0}^{n-1} |\xi^{c_i} - \xi^{a_i}|^2}, \frac{\mu}{\sigma}\right). \tag{4.15}$$

More generally let $E[\rho_r] = 0$ and $E[\rho_r \rho_s^*] = R_{rs}$ be the correlation between ρ_r and ρ_s. These correlations can be measured or calculated using a given channel model. The metric $\Lambda(\mathbf{a})$ is now a sum of correlated Chi-square variables. The characteristic function of $\Lambda(\mathbf{a})$ is given by [46]

$$\phi_\Lambda(\omega) = \frac{1}{\det\left[I - j\mathbf{R}\omega\right]}. \tag{4.16}$$

where $\mathbf{R} = [R_{rs}]$ and

$$R_{rs} \triangleq \begin{cases} X_{rs}\left|\xi^{c_r} - \xi^{b_r}\right|^2 + \sigma^2 & r = s \\ X_{rs}\left(\xi^{c_r} - \xi^{b_r}\right)\left(\xi^{-c_s} - \xi^{-b_s}\right) & r \neq s. \end{cases} \tag{4.17}$$

Using the Gil-Pelaez lemma [23], we have

$$\Pr\left[\Lambda\left(\mathbf{a}\right) < \mu^2\right] = \frac{1}{2} - \int_{-\infty}^{\infty} \frac{e^{-j\omega\mu^2}}{\det\left[I - j\mathbf{R}\omega\right] j2\pi\omega} d\omega \tag{4.18}$$

Therefore, for the more general case where $\rho_i \quad (i = 0, \cdots, n-1)$ are zero-mean complex random variables (Rayleigh fading), the average complexity of the proposed algorithm is given by

$$E\left(T\right) = \sum_{\mathbf{a} \in GS(n)} \frac{1}{2} - \int_{-\infty}^{\infty} \frac{e^{-j\omega\mu^2}}{\det\left[I - j\mathbf{R}\omega\right] j2\pi\omega} d\omega. \tag{4.19}$$

These expressions can be evaluated for a given code and channel state.

4.5 Conclusion

In this chapter, we extended the application of our low-complexity decoding algorithms to QAM and to differential MDPSK transceivers. We used computer simulation to compare the BER performance as well as the complexity of our decoding algorithm with existing decoders. Finally, we analyzed the complexity of our proposed algorithm and developed an analytical approximation.

Chapter 5

Design of Low Complexity Optimizer for the Partial Transmit Sequence Technique

In Chapter 2, we described the problem of high peak-to-average-power ratio (PAPR) in orthogonal frequency division multiplexing (OFDM) signals and we classified the existing PAPR reduction techniques. Partial transmit sequence (PTS) is a promising technique for PAPR reduction in OFDM systems. Optimal PTS weight factor computing via exhaustive search requires exponential complexity in the number of sub-blocks; consequently, many suboptimal strategies have been developed to date. In this chapter, for the first time, we give an algorithm for computing the optimal PTS weights. It has substantially lower complexity compared to exhaustive search.

5.1 Overview of PTS

OFDM is emerging as a key technology for 4th generation (4G) cellular networks. It is increasingly held that OFDM gives an improved downlink per-

formance for 4G [59]. However, a drawback is the potentially high PAPR of OFDM signals. Many PAPR reduction techniques have been developed such as block coding based on Golay sequences (with dual capabilities of error correction and peak reduction) [15]. Another such technique that is distortion-free and of low redundancy is partial transmit sequences (PTS) [67, 75].

Fig. 2.6 shows the block diagram of a PTS transmitter. Let $\mathbf{D} = [D_1, \cdots, D_n]^T$ be a block of n symbols being transmitted where each symbol is modulated to one of the carrier frequencies $\{f_i, i = 1, \cdots, n\}$. In OFDM, the n subcarriers are chosen to be orthogonal ($f_i = i\Delta f$) where $\Delta f = 1/nT$ and T is the signal period. The complex envelope of the transmit signal is

$$d(t) = \frac{1}{\sqrt{n}} \sum_{i=1}^{n} D_i e^{j2\pi f_i t} \quad 0 \le t < nT \tag{5.1}$$

where $j = \sqrt{-1}$. The PAPR of the OFDM signal $d(t)$ is defined as

$$\text{PAPR} = \frac{\max |d(t)|^2}{E\left[|d(t)|^2\right]}. \tag{5.2}$$

Note that $E\left[|d(t)|^2\right] = 1$ for unitary signal constellations. To better approximate the PAPR (5.2), (5.1) can be oversampled for generating Ln samples where $L > 1$ is the oversampling factor. When $L = 1$, Nyquist-rate sampling is obtained. These samples can be computed by using appropriate zero-padding and using an inverse fast Fourier transform (IFFT).

In the PTS approach, $\mathbf{D}$ is divided into M disjoint sub-blocks $\mathbf{D}_m$ ($1 \le m < M$) of length U where $n = MU$ for some integers M and U. Now suppose that for $m = 1, \cdots, M$, $[R_{m,1}, \cdots, R_{m,Ln}]^T$ is the zero-padded IFFT of $\mathbf{D}_m$. PTS combines the phase-rotated version of these in order to minimize the

PAPR. The signal samples at the PTS output can be written as

$$\mathbf{d}' = \underbrace{\begin{bmatrix} R_{1,1} & R_{1,2} & \cdots & R_{1,M} \\ R_{2,1} & R_{2,2} & & \\ \vdots & & \ddots & \\ R_{Ln,1} & & & R_{Ln,M} \end{bmatrix}}_{\mathbf{R}} \cdot \underbrace{\begin{bmatrix} b_1 \\ b_2 \\ \vdots \\ b_M \end{bmatrix}}_{\mathbf{b}} \tag{5.3}$$

where $\mathbf{d}' = [d'_1, \cdots, d'_{Ln}]$ is the block of optimized signal samples. Let $\mathbf{R}_k$ represent the k-th row of the matrix $\mathbf{R}$. Then each element of $\mathbf{d}'$ can be expressed as

$$d'_k = \begin{bmatrix} R_{k,1} & R_{k,2} & \cdots & R_{k,M} \end{bmatrix} \cdot \begin{bmatrix} b_1 \\ b_2 \\ \vdots \\ b_M \end{bmatrix} = \mathbf{R}_k \cdot \mathbf{b}. \tag{5.4}$$

The optimization problem is to find optimum phases b_i according to

$$\{b_1^*, \cdots, b_M^*\} = \underbrace{\arg\min}_{\{b_1, \cdots, b_M\}} \left(\max_{1 \le k < Ln} \left| \sum_{m=1}^{M} b_m R_{k,m} \right| \right) \tag{5.5}$$

where $b_i \in P = \{e^{\frac{j2\pi k}{q}}, k = 0, \cdots, q-1\}$. The last phase factor can be fixed ($b_M = 1$) without loss of generality. Therefore, q^{M-1} distinct possible vectors $\mathbf{b}$ should be tested to solve (5.5). Accordingly, the computational complexity increases exponentially with the number of sub-blocks. In the next section, we propose a new optimization algorithm that solves (5.5) with substantially lower complexity.

Our new algorithm is motivated by the shortest vector problem (SVP) in a lattice. An M-dimensional lattice is the set of vectors (lattice points)

$\{\mathbf{Ab} \mid b_i \in \mathbb{Z}\}$, where $\mathbf{b} = (b_1, \ldots, b_M)'$ and the columns of matrix $\mathbf{A} \in \mathbb{R}^{N \times M}$ are called the *basis* for the lattice. The SVP requires finding the shortest non-zero vector in the lattice. The length can be measured in any l_p ($p \geq 1$) norm. The l_p norm of a vector $\mathbf{d} = (d_1, d_2, \ldots, d_n)$ is defined to be $||\mathbf{d}||_p = (\sum |d_i|^p)^{\frac{1}{p}}$ and $||\mathbf{d}||_\infty = \max_i |d_i|$. Fincke and Phost [21] develop an efficient algorithm for SVP in l_2 (i.e., Euclidean distance) by enumerating all the lattice points inside a sphere centered at the origin. Accordingly, sphere decoding has wide application in communication problems (see [47] for a detailed survey). The signal vectors (5.3) can be readily interpreted as lattice points generated by $\mathbf{R}$. However, note that (5.5) is equivalent to the SVP in l_∞ norm. As such, the original Fincke Phost sphere decoder (FPSD) cannot be directly apply to our problem at hand. Nevertheless, the basic premise of FPSD, which is to generate lattice points $\mathbf{d}$ for which $||\mathbf{d}||_2 \leq \mu$, can be adapted; consequently, only lattice points for which $||\mathbf{d}||_\infty \leq \mu$ are generated, but this is equivalent to $|d_k| \leq \mu \; \forall k$.

5.1.1 Existing Optimizers

Optimal PTS weight factor computing via exhaustive search requires exponential complexity in the number of subblocks; consequently, many suboptimal strategies have been developed to date. The suboptimal strategies include the following. The iterative flipping algorithm (FA) [12] has complexity linearly proportional to the number of subblocks and each phase factor is individually optimized regardless of the optimal value of other phases. A neighborhood search is proposed in [26] using gradient descent search. Reference [30] uses dual layered phase sequencing to reduce the complexity at the price of PAPR performance degradation. In [75] a suboptimal strategy is developed by modifying the problem into an equivalent problem of minimization of the sum of

phase-rotated vectors. An initial set of phase vectors are computed by reducing the peak amplitude of each sample and the best phase vector of the set is chosen as the final solution. Finally, [10] gives an orthogonal projection-based approach for computing PTS phase factors.

5.2 New FPSD-based PTS Optimizer

Let $\mathbf{d}' = [d'_1, \cdots, d'_{Ln}]$ be defined as in (5.3) and let $\mathbf{R}_k$ represent the k-th row of the matrix $\mathbf{R}$. According to (5.4) each element of $\mathbf{d}'$ can be expressed by $d'_k = \mathbf{R}_k \cdot \mathbf{b}$. In order to find the PAPR of the OFDM signal, the amplitude of d'_k is computed according to

$$\begin{aligned} |d'_k|^2 &= {d'_k}^H \cdot d'_k \\ &= \mathbf{b}^H \cdot \mathbf{R}_k^H \cdot \mathbf{R}_k \cdot \mathbf{b} \\ &= \mathbf{b}^H \cdot \underbrace{\left[\mathbf{R}_k^H \cdot \mathbf{R}_k + \alpha^2 \mathbf{I}\right]}_{\mathbf{A}_k} \cdot \mathbf{b} - \alpha^2 \mathbf{b}^H \cdot \mathbf{b} \\ &= \mathbf{b}^H \cdot \mathbf{A}_k \cdot \mathbf{b} - \alpha^2 M. \end{aligned} \tag{5.6}$$

where α is an arbitrary nonzero real number and $(\cdot)^H$ denotes conjugate transpose. To complete the optimization, we first prove the following theorem.

Theorem : Let $\mathbf{R}_k$ be defined as in (5.4) and let $\mathbf{I}$ be the unity matrix. Then the matrix $\mathbf{A}_k = \mathbf{R}_k^H \cdot \mathbf{R}_k + \alpha^2 \mathbf{I}$ is a positive definite matrix.

Proof: Let $\mathbf{s} = [s_1, \cdots, s_M]$ be a nonzero vector in $\mathbf{R}^M$. We have

$$
\begin{aligned}
&\mathbf{s}^H \cdot \mathbf{A}_k \cdot \mathbf{s} \\
&= \begin{bmatrix} s_1 & \cdots & s_M \end{bmatrix} \cdot \begin{bmatrix} R_{1,1} + \alpha^2 & \cdots & R_{1,M} \\ R_{2,1} & & \\ \vdots & \ddots & \\ R_{M,1} & & R_{M,M} + \alpha^2 \end{bmatrix} \cdot \begin{bmatrix} s_1 \\ \vdots \\ s_M \end{bmatrix} \\
&= \begin{bmatrix} \alpha^2 s_1^H + R_{1,k}^H \sum_{i=1}^{M} s_i^H R_{i,k} & \cdots & \alpha^2 s_M^H + R_{M,k}^H \sum_{i=1}^{M} s_i^H R_{i,k} \end{bmatrix} \cdot \begin{bmatrix} s_1 \\ \vdots \\ s_M \end{bmatrix} \\
&= \alpha^2 \sum_{i=1}^{M} \|s_i\|^2 + \sum_{j=1}^{M} \sum_{i=1}^{M} s_i^H R_{i,k}^H s_j R_{j,k} \\
&= \alpha^2 \sum_{i=1}^{M} \|s_i\|^2 + \sum_{i=1}^{M} \|s_{i,k} R_{i,k}\|^2 > 0
\end{aligned} \tag{5.7}
$$

Eqn. (5.7) shows that $\mathbf{s}^H \cdot \mathbf{A}_k \cdot \mathbf{s} > 0$ for all $\mathbf{s} \in \mathbf{R}^M$. Accordingly, the $M \times M$ matrix $\mathbf{A}_k$, since it is positive-definite due to the addition of $\alpha^2\mathbf{I}$, can be Cholesky factorized as

$$\mathbf{A}_k = \mathbf{Q}_k^H \cdot \mathbf{Q}_k \tag{5.8}$$

where $\mathbf{Q}_k$ is an upper-triangular matrix. Substituting $\mathbf{A}_k$ from (5.8) into (5.6) gives

$$
\begin{aligned}
|d_k'|^2 &= \mathbf{b}^H \cdot \mathbf{Q}_k{}^H \cdot \mathbf{Q}_k \cdot \mathbf{b} - \alpha^2 M \\
&= \|\mathbf{Q}_k \cdot \mathbf{b}\|^2 - \alpha^2 M
\end{aligned} \tag{5.9}
$$

where the signal sample is now a function of the phase vector $\mathbf{b}$. Now suppose that we want to limit the PAPR (5.2) to $\mu^2 E\left[|d(t)|^2\right]$ for some positive number μ. So the candidate phase vectors can be generated from (5.9) subject to the

following constraint:

$$\left\| \begin{bmatrix} Q^k_{1,1} & \cdots & Q^k_{1,M} \\ 0 & Q^k_{2,2} & \vdots \\ \vdots & \ddots & \\ 0 & 0 & Q^k_{M,M} \end{bmatrix} \cdot \begin{bmatrix} b_1 \\ b_2 \\ \vdots \\ b_M \end{bmatrix} \right\|^2 < \mu^2 + \alpha^2 M \tag{5.10}$$

for $1 \leq k \leq Ln$. Sphere decoding only searches among those candidates that lie inside the sphere of radius $\mu^2 + \alpha^2 M$ and therefore, reduces the complexity. We rewrite (5.10) as

$$\sum_{v=1}^{M} \left| \sum_{u=v}^{M} Q^k_{v,u} b_u \right|^2 < \mu^2 + \alpha^2 M \ , \ 1 \leq k \leq Ln. \tag{5.11}$$

In order to satisfy (5.11), the following set of inequalities should be satisfied for $1 \leq k \leq Ln$:

$$\left| Q^k_{M,M} b_M \right|^2 < \mu^2 + \alpha^2 M, \tag{5.12a}$$

$$\sum_{v=M-1}^{M} \left| \sum_{u=v}^{M} Q^k_{v,u} b_u \right|^2 < \mu^2 + \alpha^2 M, \tag{5.12b}$$

$$\sum_{v=M-2}^{M} \left| \sum_{u=v}^{M} Q^k_{v,u} b_u \right|^2 < \mu^2 + \alpha^2 M, \tag{5.12c}$$

$$\vdots$$

$$\sum_{v=1}^{M} \left| \sum_{u=v}^{M} Q^k_{v,u} b_u \right|^2 < \mu^2 + \alpha^2 M. \tag{5.12d}$$

Note that (5.12a) contains b_M only and (5.12b) contains b_{M-1} and b_M only and so on. We fix $b_M = 1$ without loss of generality. However, (5.12a) gives a constraint on parameter μ. We use (5.12b) and $b_M = 1$ to generate candidates for b_{M-1}. These candidates and (5.12c) are used to generate candidates for

b_{M-2}. This process is repeated until the candidates for the whole phase vector $\mathbf{b}$ are generated. The resulting number of candidates is substantially smaller than q^{M-1}. Therefore, the search space is reduced, instead of exhaustively searching all the q^{M-1} phase vectors. This significantly reduces complexity.

5.2.1 Simulation Results

Computer simulation is used to compare the performance of our algorithm with that of exhaustive search and the suboptimal FA [12]. We simulate OFDM signals with 512 8-PSK subcarriers. The number of subblocks in PTS is 8 ($M = 8$). The PTS phase factors are chosen from $P = \{+1, -1\}$. The parameter α is arbitrarily chosen to be $\sqrt{M}$ for the simulation.

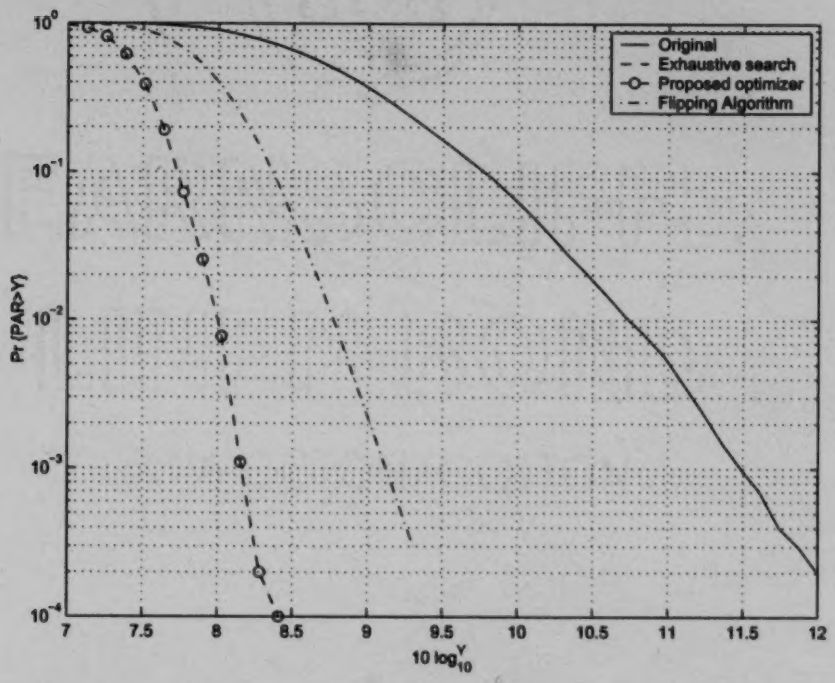

Figure 5.1: CCDF of the PAPR for exhaustive search, proposed optimizer and flipping algorithm

Fig. 5.1 compares the complementary cumulative density functions (CCDF's). Our proposed algorithm gives an additional 1 dB reduction compared to the FA. Note also that both the proposed algorithm and exhaustive search perform identically, verifying that the proposed algorithm is optimal.

Fig. 5.2 shows the optimization time versus the square of the constructed sphere radius (μ^2). The time is normalized with respect to the exhaustive search time. The results show that the complexity of the proposed optimizer decreases with the decrease in μ and in the worst-case, it is similar to the complexity of the exhaustive search. Also, when μ is small enough, the complexity is as low as the sub-optimal flipping algorithm. However, the PAPR reduction capability of the proposed algorithm is similar to that of the exhaustive search and independent of the choice of μ.

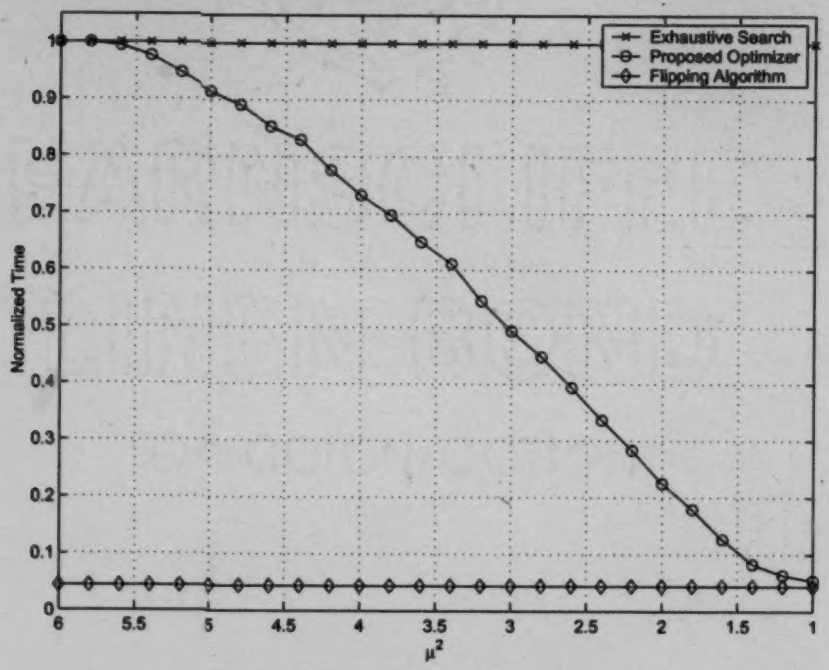

Figure 5.2: Comparison of the optimizing time required in exhaustive search, proposed optimizer and flipping algorithm

5.3 Conclusion

In this chapter, we proposed a novel algorithm for computing the PTS phase factors. Our algorithm limits the search space to only those phase vectors that guarantee that the PAPR is bounded. We extended the Fincke and Phost SD for this purpose. Computer simulation results showed that our algorithm performs with optimal PAPR reduction and with substantially lower complexity compared to exhaustive search.

Chapter 6

PAPR Reduction using Standard Array of Linear Block Codes

In Chapter 2, we mentioned that a novel PAPR reduction technique has been proposed [97] based on the standard array of linear block codes (STA). The performance of STA is comparable to that of selected mapping (SLM) in the absence of channel distortion. However, our simulations show that STA is highly sensitive to channel distortion and may perform substantially worse when symbol errors occur during transmission. In this chapter, we propose the use of a channel encoder in STA. We evaluate the performance of STA with convolutional codes and turbo-codes and show that the channel coding mitigates the sensitivity of STA to channel distortion and preserves PAPR reduction.

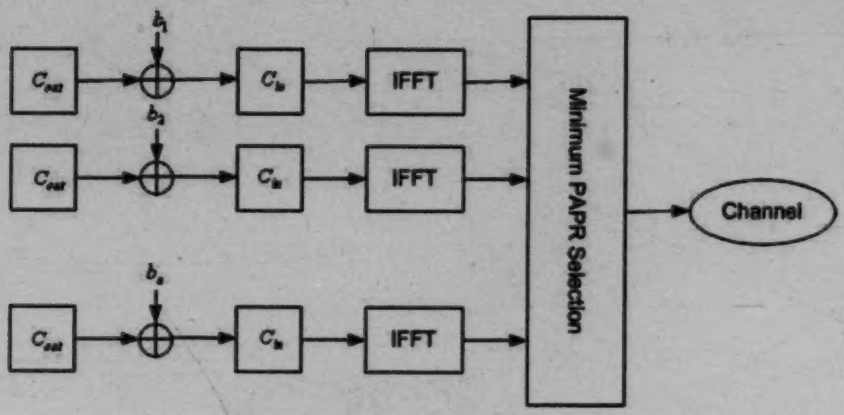

Figure 6.1: Block diagram of the STA transmitter

6.1 STA-Based OFDM Transmitter and Receiver Architecture

In an STA-based transmitter, the PAPR is reduced by generating several signals for the same information vector with different PAPR characteristics. The transmitter chooses the signal with lowest PAPR for transmission. Note that STA may be viewed as variation of SLM [60]. In STA a simple linear block code such as a Hamming code (C_{out}) scrambles the transmitted signal. The resulting signal is then added to coset leaders which have different syndromes to generate multiple OFDM signal alternatives.

Let u be the number of signals generated for PAPR reduction. The transmitted data is encoded with the outer encoder (C_{out}) and added to the coset leader vectors ($\mathbf{b}_k, k = 1, \cdots, u$) in each branch. As shown in Fig. 6.1, channel coding (C_{in}) is performed in each branch on the multiple signals. Each alternative is then modulated (*i.e.* PSK or QAM) and its IFFT transformation is computed to form an OFDM signal. Finally, the OFDM signal with lowest PAPR value is selected and transmitted across the channel.

6.2 Performance Evaluation of STA-Based OFDM Transceivers in Ideal Communications Channel

Let C be an (n, k) block code with parity-check-matrix $\mathrm{H}_{(n-k)\cdot n}$, where k is the length of the source words and n is the length of the codewords. A coset of C is defined as $\{\mathbf{c}+\mathbf{b}|\mathbf{c} \in \mathrm{C}, \mathbf{b} \notin \mathrm{C}\}$. The vector $\mathbf{b}$ is called the coset leader. Note that there are $z = 2^{n-k}$ cosets. For each coset we have [13]

$$\begin{aligned} \mathbf{s}_{(n-k)\times 1} &= \mathrm{H}_{(n-k)\cdot n} \cdot (\mathbf{c}+\mathbf{b}) \\ &= \mathrm{H}_{(n-k)\cdot n} \cdot \mathbf{c} + \mathrm{H}_{(n-k)\times n} \cdot \mathbf{b} \\ &= \mathrm{H}_{(n-k)\cdot n} \cdot \mathbf{b} \end{aligned} \tag{6.1}$$

where $\mathbf{s}_{(n-k)\times 1}$ is the syndrome. Accordingly, there are $z = 2^{n-k}$ different syndromes.

In STA, multiple signals are generated by adding different coset leaders to the encoded data. In order to recover the coset leaders in the receiver, the u coset vectors $\mathbf{b}_k$ $(k = 1, \cdots, u)$ should correspond to different syndromes. Therefore, the STA technique does not require explicit side information to be transmitted.

Let $S = \{\mathbf{s}|\mathbf{s} = \mathrm{H} \cdot (\mathbf{c}+\mathbf{b}), \forall \mathbf{c} \in \mathrm{C}, \mathbf{b} \notin \mathrm{C}\}$ be the set of all possible syndromes. Also, let $U \subseteq S$ be a subset of S with u distinct members ($u \leq 2^{n-k}$). The u different syndromes in U correspond to the u coset vectors $(\mathbf{b}_k)$ that are used in the branches of the STA transmitter. The choice of the u scrambling coset leaders has an impact on the quality of PAPR reduction and hence, it is important to choose the optimum coset leaders. However, this requires choosing u optimum coset leaders among $z = 2^{n-k}$ possible cosets.

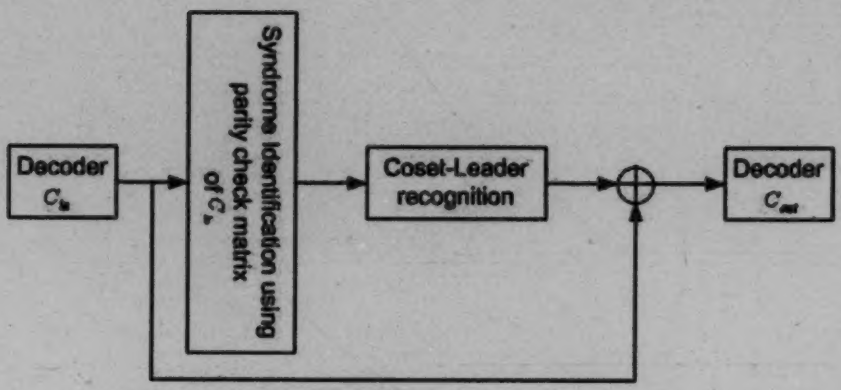

Figure 6.2: Block diagram of the STA receiver

Fig. 6.2 shows the simplified block diagram of the STA receiver. Let us first consider the case where the communication channel does not introduce any errors. In order to retrieve the message, the received vector is multiplied by the parity check matrix of the outer code C_{out} according to (6.1), which results in a syndrome vector corresponding to a unique coset vector. The original codeword is then retrieved in the receiver by subtracting the coset leader from the detected data and decoded according to C_{in} [97].

Computer simulation is used to evaluate the performance of the PAPR reduction technique. Fig. 6.3 compares the PAPR reduction performance of STA with that of SLM. It also shows the impact of the number of branches (u) on the PAPR reduction capability of the system. The transceiver is simulated for three values of u ($u = 4, 16, 64$). Data vectors are coded with a Hamming code to codewords of length $n = 256$. With $u = 4$ and $u = 16$, more than 2.3 dB and when $u = 16$, more than 3.6 dB performance improvement is respectively achieved when 0.1% PAPR is considered. Also the simulation shows that STA has slightly better PAPR reduction capability than original SLM [97]. This may be due to the better scrambling capability of linear block codes. The difference becomes more significant when the number of

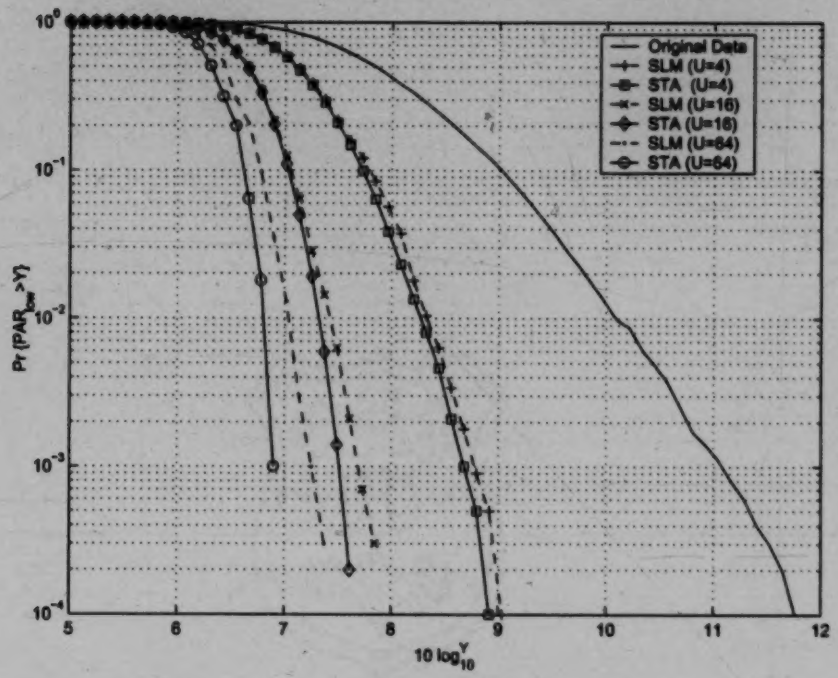

Figure 6.3: CCDF of PAPR for STA transmitter with different number of branches

branches increases (*i.e.* $u = 64$). However, since using 64 branch requires 64 FFT modules in the transmitter, and also since the PAPR is not significantly reduced compared to when $u = 16$ branches are implemented, the choice of $u = 16$ branches appears to be a good choice.

We next study the PAPR reduction performance of the STA technique with a nonlinear high-power amplifier (HPA). The impact of different levels of nonlinearity on the power spectral density (PSD) of the OFDM signal is shown in Fig. 6.4 where the HPA nonlinearity is modelled as a soft-limiter allowing input back-offs (IBO) of 6 and 8 dB and where STA is implemented with 16 branches. Simulation shows that when OFDM without PAPR reduction is passed through the nonlinear HPA, the level of out-of-band radiation (OBR)

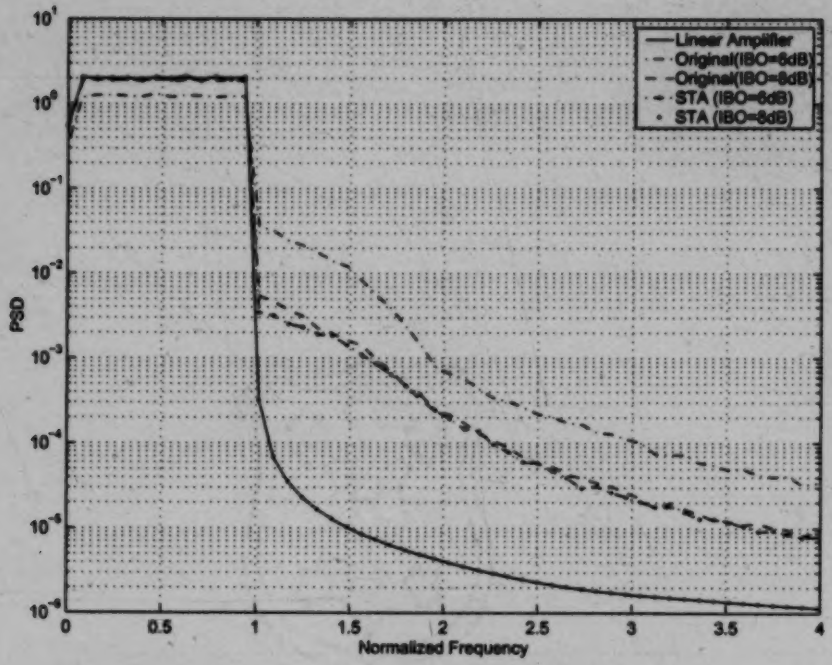

Figure 6.4: PSD of the OFDM signals with and without STA and with linear and nonlinear HPA

for an IBO of 6 and 8 is 30 and 20 dB more than that which occurs with the linear amplifier, respectively. However, when STA is used to reduce the PAPR of the signals, only 20 dB more OBR is observed for IBO = 6 dB and when IBO = 8 dB is considered, the resulting OBR is negligible. This improvement is due to the fact that the STA-based transmitter, on average, reduces the PAPR of the transmitted signals and fewer OFDM symbols are distorted by the HPA nonlinearity. Note that since the HPA with IBO = 8 dB introduces no significant distortion, design of HPAs with more than 8 dB back-off does not yield any further significant improvement. Note that due to the similarity between SLM and STA, similar results are expected for SLM.

6.3 STA-Based OFDM Transceivers in Non-Ideal Channels

In practice, communication channels distort the transmit signal by additive noise or by multiplicative fading. Although STA reduces PAPR well, STA decoding is susceptible to channel distortion and therefore the use of high performance channel encoding in STA transceivers is vital.

Let $\mathbf{x} = \mathbf{c} + \mathbf{b}$ be the transmitted data and let $\mathbf{s}$ be its corresponding syndrome according to (6.1). Also let $\mathbf{e}_n$ be additive white Gaussian noise corresponding to the channel distortion. The received signal $\mathbf{y}$ can be written as

$$\mathbf{y} = \mathbf{x} + \mathbf{e}_n. \tag{6.2}$$

Multiplying the received vector $\mathbf{y}$ by the parity-check matrix $H_{(n-k)\cdot n}$ gives the syndrome $\acute{\mathbf{s}}$ as

$$\begin{aligned}
\acute{\mathbf{s}} &= H_{(n-k)\cdot n} \cdot \mathbf{y} \\
&= H_{(n-k)\cdot n} \cdot (\mathbf{x} + \mathbf{e}_n) \\
&= H_{(n-k)\cdot n} \cdot \mathbf{x} + H_{(n-k)\cdot n} \cdot \mathbf{e}_n \\
&= \text{Syndrome}(\mathbf{c} + \mathbf{b}) + \text{Syndrome}(\mathbf{e}_n) \\
&= \mathbf{s} + \mathbf{s}_{\text{error}}
\end{aligned} \tag{6.3}$$

Since $\acute{s} \in S$ by definition, it corresponds to a valid coset vector different from $\mathbf{b}$ and therefore the decoder decodes the source code $\mathbf{c}$ to a vector $\mathbf{c}' \neq \mathbf{c}$. Note that even one bit error results in erroneous bits in the decoded data and loss of information. Therefore, use of an efficient channel encoder C_{in} is crucial for STA transceivers. Two channel coding techniques are reviewed next and their

impact on the performance of the transceiver is investigated.

6.4 Impact of Channel Encoding on STA Transceivers

As mentioned in the previous sections, channel encoding in STA transceiver systems is required in practice. In the following, two high-performance and widely-used codes, namely turbo-codes and convolutional codes, are considered as the inner encoder (C_{in}) for STA and their performance under several non-ideal conditions is investigated.

6.4.1 STA-Based Transceiver Using Turbo-Codes

Turbo coding is used as the inner code (C_{in}) for the transceiver structure of Fig. 6.1. The input data of length 124 bits are randomly generated and encoded using the modified Hamming code $H_{128\times124}$. Random search is used to generate the $u = 2^4$ coset vectors with distinct syndromes. Then, the coset vectors are added to the coded data in each branch. The resulting 128-bit vectors are then encoded using the turbo-code comprised of recursive systematic convolutional codes. The turbo-code uses the generating polynomials G_5 and G_7 with two-bit memory as introduced in [7]. A code rate of 1/3 is initially obtained, which can be increased to 1/2 by puncturing. Random interleaving is used in each frame and the resulting data vector is modulated with BPSK. The signal being transmitted is OFDM-modulated using a 512 bit IFFT. An oversampling rate of 4 is used in order to precisely estimate the maximum PAPR of the OFDM signal. The transmitter selects a codeword with lowest PAPR among the u possible OFDM signals and transmits it across an AWGN channel.

The BER performance of the transceiver using turbo coding is also evaluated. Fig. 6.5 shows the bit error rate of the system in an AWGN channel. The

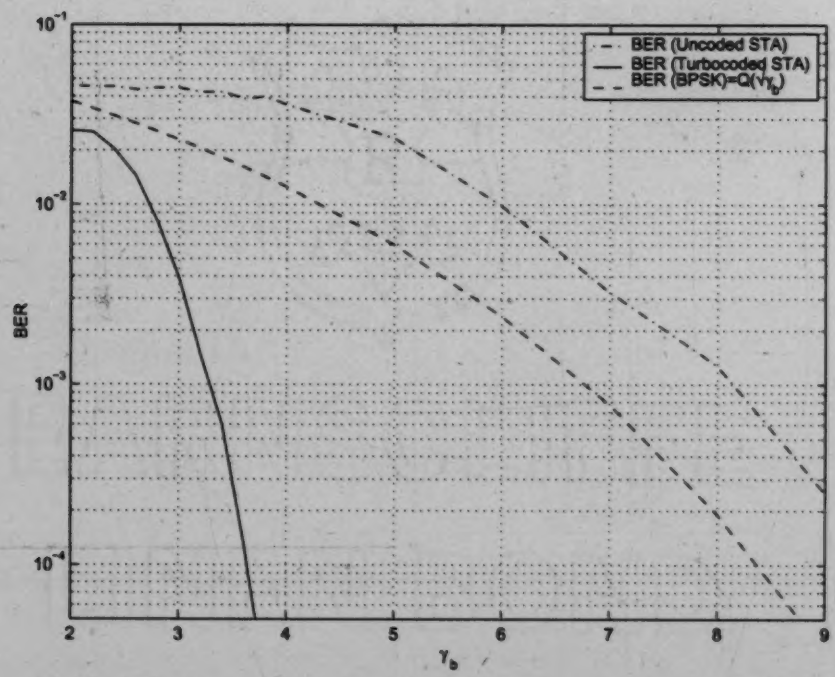

Figure 6.5: Bit Error Rate of an STA-Based Transceiver over an AWGN channel with a turbo code as the outer code

first curve (uncoded STA) shows the performance of the STA without channel coding. Due to the structure of the STA transceiver, even a few erroneous bits translate into burst errors in the receiver when no channel coding is used. In order to highlight this deficiency, the BER performance of the uncoded transceiver is compared with that of a single carrier BPSK. Fig. 6.5 shows that the uncoded transceiver performs more than 2 dB worse than the single carrier BPSK. Finally, the result for Turbocoded STA shows that employing the turbo code mitigates the problem and significantly reduces the effect of channel impairments in addition to yielding improved low PAPR.

6.4.2 STA-Based Transceiver Using Convolutional Codes

In this section, we investigate the performance of the STA transceiver when a convolutional code is used as the channel encoder. Convolutional codes are considered for the STA system due to the simplicity of their decoding using the Viterbi algorithm and their good BER performance.

Fig. 6.6 shows the simulation results for the complementary cumulative distribution function (CCDF) of PAPR for OFDM vectors generated in the STA transmitter. The CCDF of OFDM vectors with different lengths are compared for both uncoded and convolutional coded BPSK. Note that the CCDF of the uncoded vector coincides with that of the convolutional coded vector of the same length. This shows that the convolutional codes have similar PAPR characteristics compared to the uncoded vectors. Therefore, incorporating the convolutional codes in the STA transceiver does not reduce the PAPR reduction performance of the STA.

Fig. 6.7 shows the BER performance of the OFDM system with linear and nonlinear HPAs. Data is sent in blocks of 512 bits and modulated by BPSK. The BER performance is evaluated with respect to the different levels

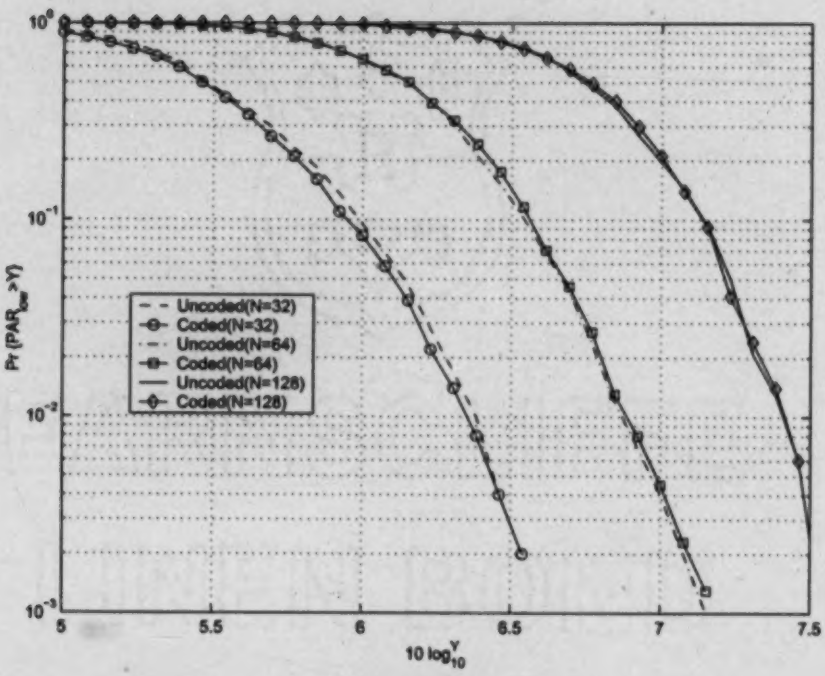

Figure 6.6: CCDF of PAPR of OFDM signals using convolutional coding and using uncoded BPSK vectors of length 32, 64 and 128

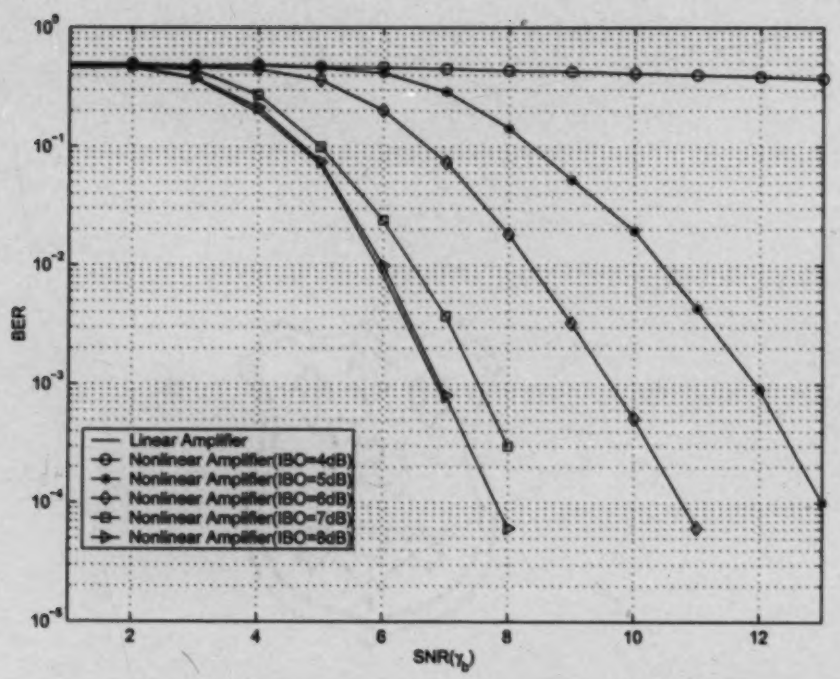

Figure 6.7: BER performance of STA transceiver without a nonlinear HPA and with nonlinear HPAs with convolutional code as outer code

of nonlinearity. Note that due to the PAPR reduction of the STA, the BER performance of the system with an 8 dB input back-off is almost the same as that of the system with a linear amplifier.

The PSD and the BER performance of other STA-based OFDM transceivers are investigated next. In this instance a soft non-linear HPA is used and frequency non-selective Rayleigh fading model is assumed for the communication channel. Data is coded in blocks of length 128 and modulated with QPSK. Fig. 6.8 depicts the effect of a nonlinear HPA on the power spectra of OFDM signals. Note that when PAPR reduction is not employed, about 20 dB and 30 dB out-of-band radiation is observed for 6 and 8 dB IBO in the HPA, respectively. However, when STA is employed, less than 30 dB out-of-band radiation

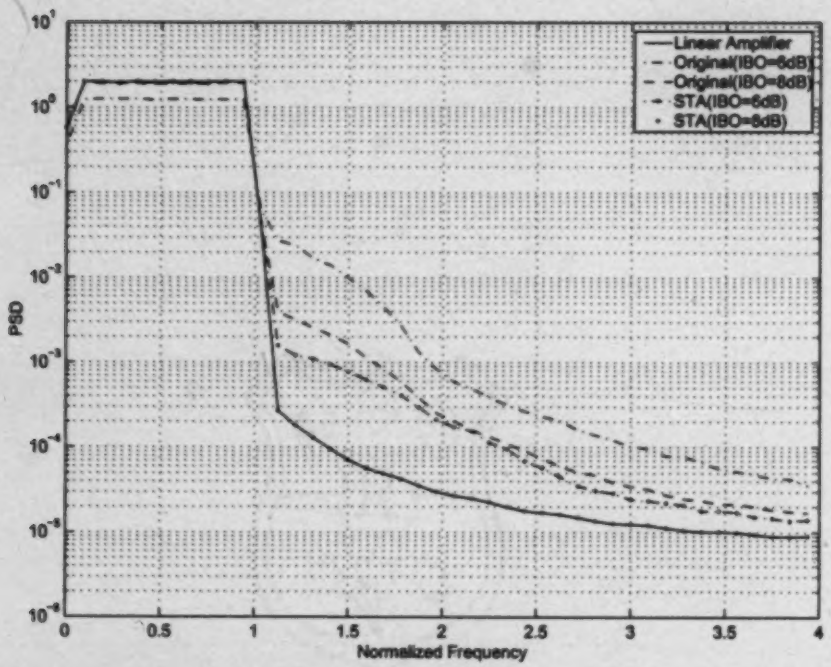

Figure 6.8: PSD of the OFDM signals with and without STA and with linear and nonlinear HPA with QPSK and $n = 128$.

is observed when the IBO of the nonlinear HPA is 6 dB. Moreover, when an HPA with 8 dB IBO is used, the IBO is almost negligible.

Fig. 6.9 shows the BER performance of the transceiver when perfect channel estimation is considered. The results show that using the STA, only 3 dB SNR reduction is observed at a BER of 10^{-2} with IBO = 6 dB compared to when a linear amplifier is employed. Also, nearly 10 dB SNR degradation is observed with IBO = 8 dB.

6.5 Conclusion

In this chapter, PAPR reduction based on the standard array of a linear block codes (STA) was studied and its performance was compared to the perfor-

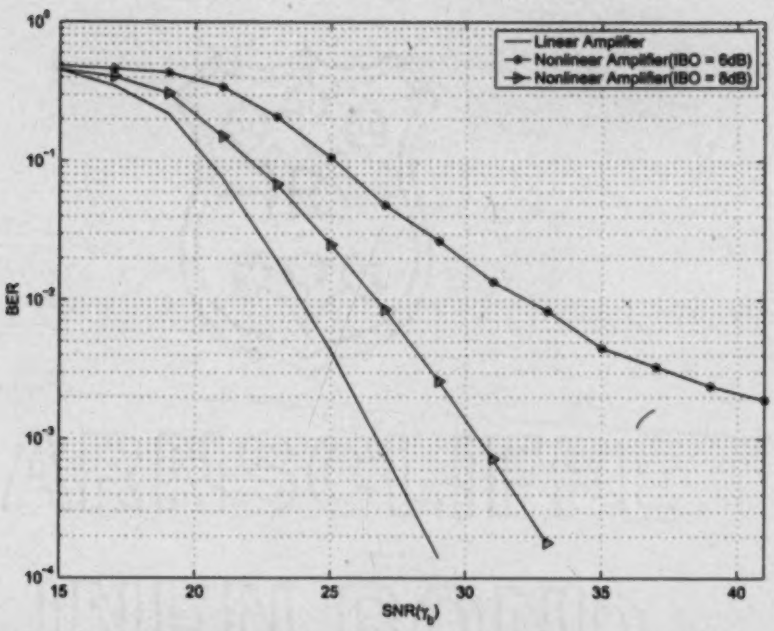

Figure 6.9: BER performance of STA transceiver without and with nonlinear HPA with different levels of nonlinearity in Rayleigh fading channel. QPSK modulation is used for data vectors of length $n = 128$.

mance of the selected-mapping technique (SLM). Simulation results showed that STA is highly sensitive to channel distortion and channel encoding needs to be included in the STA transceiver. Finally, the impact of turbo codes and convolutional codes on the performance of the STA was investigated and computer simulation was used to evaluate the performance of the transceivers.

Chapter 7

Conclusion

Increasing demand for high data-rate wireless communications has led to the investigation of more spectrally efficient solutions. OFDM has thus gained an increasing interest due to its tolerance to multi-path fading and its bandwidth efficiency. However, the high PAPR of the OFDM signals is a drawback for portable applications and hence, several techniques including the use of power-limited sequences such as Golay sequences have been shown to be promising solutions. The design of a low-complexity maximum-likelihood decoder for Golay sequences is a challenging problem.

In Chapter 1, the problem of PAPR reduction and the motivation of our work was introduced. In Chapter 2, we reviewed sub-optimal and optimal PAPR reduction techniques and related works developed in the literature. Several PAPR reduction techniques were discussed in this chapter and basic concepts of OFDM and mathematical models of the channel were introduced.

In Chapter 3, we developed efficient ML decoders for Golay sequences based on the principle of sphere decoding. We adapted the key idea of sphere decoding to limit the search space to a limited number of points in a multi-dimensional sphere centered around the received signal. Also, further im-

provements were introduced to the algorithm by proposing improved lower bounds.

In Chapter 4, we extended the application of our proposed algorithms to QAM and MDPSK-OFDM transceivers. Measures of complexity were also developed in this chapter for our proposed algorithm.

In Chapter 5, we proposed a low-complexity optimizer for the partial-transmit-sequence technique. This was done by modifying the optimization problem into an equivalent problem which is suitable for the sphere decoding algorithm. Mathematical representation of the problem was provided and following that, simulation results were presented to evaluate the performance of the proposed optimizer.

Finally, the effect of channel coding on a PAPR reduction technique based on the standard array of linear block codes was investigated in Chapter 6. We showed that turbo-codes and convolutional codes are promising solutions to mitigate the sensitivity of the STA transceivers to channel non-idealities. It was also shown that turbo-codes and convolutional codes can enhance the BER performance of the STA transceiver without reducing the PAPR reduction performance.

The area of wireless communications is a rapidly growing field. New technologies are emerging to achieve high throughput with low complexity. OFDM is expected to play a major role in such technologies. For instance, it is believed that OFDM gives an improved downlink performance for 4G [59]. This motivates future improvements to the results of this thesis. A few suggestions for the future work include the following:

1. This thesis introduces a novel decoder and optimizer for OFDM transceivers. Efficient hardware implementation of these algorithms has not yet been developed. Therefore, investigating efficient VLSI structures to represent

the algorithms in hardware can be a challenging problem.

2. In Chapter 5, we proposed a low complexity optimizer for the partial transmit sequence system. Several sub-optimal variations of the proposed algorithms can be derived. It is expected that sub-optimal approaches exist that yield even lower complexity with negligible performance degradation.

3. Incorporating OFDM in the emerging 4G technology encourages the design of a test-bed that could evaluate the performance of the proposed algorithms in 4G compatible transceivers. This could open a wide area of interesting research in both wireless communications and hardware design.

Bibliography

[1] K.R. Panta, J. Armstrong. Effects of clipping on the error performance of OFDM in frequency selective fading channels. *IEEE Trans. Wirel. Commun.*, 3:668 – 671, March 2004.

[2] E. Agrell, T. Eriksson, A. Vardy, and K. Zeger. Closest point search in lattices. *IEEE Trans. Inform. Theory*, 48:2201–2214, August 2002.

[3] J. Armstrong. Peak-to-average power reduction for OFDM by repeated clipping and frequency domain filtering. *IEE Elect. Lett.*, 38(5):246–247, February 2002.

[4] B. Tarokh, H. R. Sadjadpour. Construction of OFDM M-QAM sequences with low peak-to-average power ratio. *IEEE Trans. Commun.*, 51(1):25–28, January 2003.

[5] P. Banelli. Theoretical analysis and performance of OFDM signals in nonlinear fading channels. *IEEE Trans. Commun.*, 2(2):284–293, March 2003.

[6] P. Banelli and S. Cacopardi. Theoretical analysis and performance of OFDM signals in nonlinear AWGN channels. *IEEE Trans. Commun.*, 48(3):430–441, March 2000.

[7] C. Berrou, A. Glavieux, and P. Thitimajshima. Near shannon limit error-correcting coding and decoding: Turbo-codes. 1. In *IEEE ICC*, volume 2, pages 1064–1070, Geneva., 1993. IEEE.

[8] S. Boyd. Multitone signals with low crest factors. *IEEE Trans. Circuits Syst.*, CAS-33(10):1018–1022, October 1986.

[9] M. Breiling, S. Müller–Weinfurtner, and J. Huber. SLM peak–power reduction without explicit side information. *IEEE Commun. Lett.*, 5(6):239–241, 2001.

[10] H. Chen and G. J. Pottie. An orthogonal projection-based approach for PAR reduction in OFDM. *IEEE Commun. Lett.*, 6(5):169–171, May 2002.

[11] C. V. Chong and V. Tarokh. A simple encodable/decodable OFDM QPSK code with low peak-to-mean envelope power ratio. *IEEE Trans. Inform. Theory*, 47(7):3025–3029, November 2001.

[12] L. J. Cimini and N. R. Sollenberger. Peak-to-average power ratio reduction of an OFDM signal using partial transmit sequences. *IEEE Commun. Lett.*, 4(3):511–515, Mar. 1999.

[13] G.C. Clark and John B. Cain. *Error-Correction Coding for Digital Communications*. Plenum, New York, 1981.

[14] M. O. Damen, H. El Gamal, and G. Caire. On maximum-likelihood detection and the search for the closest lattice point. *IEEE Trans. Inform. Theory*, 49:2389 – 2402, October 2003.

[15] J. A. Davis and J. Jedwab. Peak-to-mean power control in OFDM, Golay complementary sequences, and Reed-Muller codes. *IEEE Trans. Inform. Theory*, 45(7):2397–2417, November 1999.

[16] E. Viterbo and J. Boutros. A universal lattice code decoder for fading channels. *IEEE Trans. Inform. Theory*, 45(5):1639–1642, July 1999.

[17] I. J. Fair, W. D. Grover, W. A. Kryzmien, and R. I. MacDonald. Guided scrambling: a new line coding technique for high bit rate fiber optic transmission systems. *IEEE Trans. Commun.*, 39(2):289–297, February 1991.

[18] I.J. Fair, Q. Wang, and V. K. Bhargava. Polynomials for guided scrambling line codes. *IEEE Journal on Selected Areas in Commun.*, 13(3):499–509, April 1995.

[19] I.J. Fair, Q. Wang, and V. K. Bhargava. Characteristics of guided scrambling encoders and their coded sequences. *IEEE Trans. Inform. Theory*, 43(1):342–347, January 1997.

[20] K. Fazel and S. Kaiser. Analysis of non-linear distortions on MC-CDMA. In *IEEE ICC*, volume 2, pages 1028–1034. IEEE, June 1998.

[21] U. Fincke and M. Pohst. Improved methods for calculating vectors of short length in a lattice, inlcuding a complexity analysis. *Math Computation*, 44:463–471, 1985.

[22] M. P. C. Fossorier and S. Lin. Soft-decision decoding of linear block codes based on ordered statistics. *IEEE Trans. Inform. Theory*, 41(5):1379–1396, September 1995.

[23] J. Gil-Pelaez. Note on the inversion theorem. *Biometrika*, 38:481–482, 1951.

[24] M. J. E. Golay. Complementary series. *IRE. Trans. Inform. Theory*, IT-7:82–87, April 1961.

[25] A. J. Grant and R. D. J. Van Nee. Efficient maximum likelihood decoding of Q-ary modulated Reed-Muller codes. *IEEE Commun. Lett.*, 2(5):134–136, May 1998.

[26] S. H. Han and J. H.Lee. Reduction of PAPR of an OFDM signal by partial transmit sequence technique with reduced complexity. In *IEEE GLOBECOM*, pages 1326 – 1329. IEEE, December 2003.

[27] S. H. Han and J. H. Lee. Modified selected mapping technique for PAPR reduction of coded OFDM signal. *IEEE Trans. Broadcast.*, 50(3):335–341, September 2004.

[28] B. Hassibi and H. Vikalo. On the expected complexity of sphere decoding. In *The Thirty-Fifth Asilomar Conference on Signals, Systems & Computers Conference*, pages 1051–1055. IEEE, 2001.

[29] W. S. Ho, A. S. Madhukumar, and F. Chin. Understanding the effect of phase noise in orthogonal frequency division multiplexing (OFDM). *IEEE Trans. Broadcast.*, 47(2):153–159, June 2001.

[30] W. S. Ho, A. S. Madhukumar, and F. Chin. Peak-to-average power reduction using partial transmit sequences: a suboptimal approach based on dual layered phase sequencing. *IEEE Trans. Veh. Technol.*, pages 1268–1272, April 2003.

[31] A. D. S. Jayalath. *OFDM for wireless broadband communication, Peak Power Reduction, Spectrum and Coding.* Ph.D. thesis, Dept. of Elect. and Comput. Eng., Univ. of Monash, 2002.

[32] A. D. S. Jayalath, K. Sathanandan, and C. Tellambura. OFDM with reduced peak-to-average power ratio by interleaving. In *IEEE Pacific-*

Rim Conference on Multimedia, pages 120–123, Sydney, Australia, 2000. IEEE.

[33] A. D. S. Jayalath and C. Tellambura. An adaptive PTS approach for the reduction of peak-to-average power ratio of an OFDM signal. *IEE Elect. Lett.*, 36(13):1161–1163, July 2000.

[34] A. D. S. Jayalath and C. Tellambura. Reducing the peak-to-average power ratio of an OFDM signal by interleaving. In *International Symposium on Wireless Personal Multimedia Communications*, pages 698–703, Bangkok, Thailand, 2000. IEEE.

[35] A. D. S. Jayalath and C. Tellambura. Reducing the peak-to-average power ratio of an OFDM signal through bit or symbol interleaving. *IEE Elect. Lett.*, 36(13):1161–1163, June 2000.

[36] A. D. S. Jayalath and C. Tellambura. Reducing the peak-to-average power ratio of an OFDM signal through bit or symbol interleaving. *IEE Elect. Lett.*, 36(13):1161–1163, June 2000.

[37] A. D. S. Jayalath and C. Tellambura. The use of interleaving to reduce the peak-to-average power ratio of an OFDM signal. In *IEEE GLOBECOM*, pages 82 –86, San Francisco, California, USA, 2000. IEEE.

[38] A. D. S. Jayalath and C. Tellambura. Peak-to-average power ratio reduction of an OFDM signal using data permutation with embedded side information. In *IEEE International Symposium on Circuits and Systems*, number 4, pages 562–565, Sydney, Australia, 2001. IEEE.

[39] A. D. S. Jayalath and C. Tellambura. Blind SLM receiver for PAR reduced OFDM. In *IEEE Vehicular Technology Conference*, number 1, pages 219–222. IEEE, 2002.

[40] A.D.S Jayalath and C.R.N. Athaudage. On the PAR reduction of OFDM signals using multiple signal representation. *IEEE Commun. Lett.*, 8:425 – 427, 2004.

[41] T. Jiang and G. Zhu. Nonlinear companding transform for reducing peak-to-average power ratio of OFDM signals. *IEEE Trans. Broadcast.*, 50(3):342–346, September 2004.

[42] E. A. Jones, T.A. Wilkinson, and S.K. Barton. Block coding scheme for reduction of peak-to-mean envelope power ratio of multicarrier transmission schemes. *IEE Elect. Lett.*, 30(25):2098–2099, Dec. 1994.

[43] D. Kim and G. L. Stuber. Clipping noise mitigation for OFDM by decision-aided reconstruction. *IEEE Commun. Lett.*, 3(1):4–6, January 1999.

[44] X. Li and L. J. Cimini. Effects of clipping and filtering on the performance of OFDM. In *IEEE Vehicular Technology Conference*, volume 2, pages 1634–1638, New York, NY,USA, 1997. IEEE.

[45] C. L. Liu. The effect of nonlinearity on a QPSK-OFDM-QAM signal. *IEEE Trans. Consumer Electron.*, 43(3):443–447, Aug. 1997.

[46] M. Schwartz, W. R. Bennett and S. Stein. *Communication Systems and Techniques.* McGraw-Hill, New York, 1966.

[47] W. H. Mow. Universal lattice decoding: principle and recent advances. *Wireless Communications and Mobile Computing*, 3:553–569, August 2003.

[48] H. Ochiai, M. P. C. Fossorier, and H. Imai. On decoding of block codes with peak reduction in OFDM systems. *IEEE Commun. Lett.*, 4(7):226–228, July 2000.

[49] H. Ochiai and H. Imai. MDPSK-OFDM with highly power efficient block codes for frequency selective fading channels. *IEEE Trans. Veh. Technol.*, 49(1):74–82, January 2000.

[50] H. Ochiai and H. Imai. On the clipping for peak power reduction of OFDM signals. In *IEEE GLOBECOM*, pages 731–735, San Francisco, USA, 2000. IEEE.

[51] H. Ochiai and H. Imai. Performance of the deliberate clipping with adaptive symbol selection for strictly band-limited OFDM systems. *IEEE J. Select. Areas. Commun.*, 18(11):2270–2277, November 2000.

[52] H. Ochiai and H. Imai. On the distribution of the peak-to-average power ratio in OFDM signals. *IEEE Trans. Commun.*, 49(2):282–289, 2001.

[53] H. Ochiai and H. Imai. Performance analysis of the deliberately clipped OFDM signal. *IEEE Trans. Commun.*, 2(10):89–101, January 2002.

[54] K. G. Paterson. Generalized Reed-Muller codes and power control in OFDM modulation. *IEEE Trans. Inform. Theory*, 46(1):104–120, January 2000.

[55] K. G. Paterson and A. E. Jones. Efficient decoding algorithms for generalized Reed-Muller codes. *IEEE Trans. Commun.*, 48(8):1272–1285, August 2000.

[56] R. N. Paulraj and D. Gore. *Introduction to Space-Time Wireless Communications.* Cambridge University Press, 1st edition, 2003.

[57] B. M. Popovic. Synthesis of power efficient multitone signals with flat amplitude spectrum. *IEEE Trans. Commun.*, 39:1031–1033, July 1991.

[58] J. G. Proakis. *Digital Communications.* McGraw-Hill, 4th edition, New York, 2001.

[59] M. Quan and P. Mannion. AT&T, Nortel plot 4G wireless nets, September 2000.

[60] R. W. Bäuml, R. F. H. Fischer and J. B. Huber. Reducing the peak-to-average power ratio of multicarrier modulation by selected mapping. *IEE Elect. Lett.*, 32(22):2056–2057, October 1996.

[61] C. Rapp. Effects of th HPA-nonlinearity on a 4-DPSK/OFDM signal for a digital sound bradcasting system. In *Conf. Rec. ECSC'91*, Luettich, 1991.

[62] C. Röbing and V. Tarokh. A construction of OFDM 16-QAM sequences having low peak powers. *IEEE Trans. Inform. Theory*, 47(5):2091–2094, July 2001.

[63] S. O. Rice. Mathematical analysis of random noise. *Bell Syst. Tech. J.*, 23:282–332, 1944.

[64] S. O. Rice. Statistical properties of a sine wave plus random noise. *Bell Syst. Tech. J.*, 27:109–157, 1948.

[65] H. Rohling, T. May, K. Bruninghaus, and R. Grunheid. Broad-band OFDM radio transmission for mutimedia applications. *IEEE Proc.*, 87(10):1778–1788, Oct. 1999.

[66] H. E. Rowe. Memoryless nonlinearities with gaussian inputs: Elementary results. *Bell Syst. Tech. J.*, 61:1519–1525, Sept. 1982.

[67] S. H. Müller and J. B. Huber. OFDM with reduced peak-to-average power ratio by optimum combination of partial transmit sequences. *IEE Elect. Lett.*, 33(5):368–369, February 1997.

[68] A. A. Saleh. Frequency independant and frequency dependent nonlinear models of TWT amplifiers. *IEEE Trans. Commun.*, COM-29:1715–1720, Nov. 1981.

[69] M. Sharif, M. Gharavi-Alkhansari, and B.H. Khalaj. On the peak-to-average power of OFDM signals based on oversampling. *IEEE Trans. Commun.*, 51(1):72–78, January 2003.

[70] M. Sharif and B. Hassibi. A deterministic algorithm that achieves the PMEPR of $c \log n$ for multicarrier signals. In *Proc. ICASSP' 03*, pages IV 540–543. IEEE, April 2003.

[71] M. Sharif and B.H. Khalaj. Peak to mean envelope power ratio of over-sampled OFDM signals: An analytical approach. In *IEEE ICC*, pages 1476 –1480. IEEE, 2001.

[72] S. Shepherd, J. Orriss, and S. Barton. Asymptotic limits in peak envelope power reduction by redundant coding in orthogonal frequency-division multiplex modulation. *IEEE Trans. Commun.*, 46(1):5–10, January 1998.

[73] C. Tellambura. Use of m-sequences for OFDM peak-to-average power ratio reduction. *IEE Elect. Lett.*, 33(15):1300–1301, July 1997.

[74] C. Tellambura. Computation of the continuous-time PAR of an OFDM signal with BPSK subcarriers. *IEEE Commun. Lett.*, 5(5):185–187, May 2001.

[75] C. Tellambura. Improved phase factor computation for the PAR reduction of an OFDM signal using PTS. *IEEE Commun. Lett.*, 5(4):135–137, April 2001.

[76] C. Tellambura and M. G. Parker. Relationship between Hamming weight and peak-to-mean envelop power ratio of orthogonal frequency division multiplexing. In *IEEE International Symposium on Information Theory*, page 245, 2002.

[77] R. Van Nee and G. Awater. New high-rate wireless LAN standard. *IEEE Trans. Commun.*, 37(12):82–88, Dec. 1999.

[78] R. Van Nee, G. Awater, M. Morikura, H. Takanashi, M. Webster, and K.W. Halford. New high-rate wireless LAN standards. *IEEE Commun. Mag.*, 37(12):82–88, Dec. 1999.

[79] R. Van Nee and R. Prasad. *OFDM for wireless multimedia communications*. Artech House Publishers, March 2000.

[80] R. Van Nee and A. De Wild. Reducing the peak-to-average power ratio of OFDM. In *IEEE Vehicular Technology Conference*, pages 2072–2076, New York, NY, USA, 1998. IEEE.

[81] R. D. J. Van Nee. OFDM codes for peak-to-average power reduction and error correction. In *IEEE GLOBECOM*, pages 740–744, New York, NY, USA, 1996. IEEE.

[82] C. Wang, M. Hsu, and Y. Ouyang. A low-complexity peak-to-average power ratio reduction technique for OFDM systems. In *IEEE GLOBECOM*, pages 2375–2379. IEEE, 2003.

[83] X. Wang, T. T. Tjhung, and C. S. Ng. Reduction of peak-to-average power ratio of OFDM system using a companding technique. *IEEE Trans. Broadcast.*, 45(3):303–307, Sept. 1999.

[84] X. Wang, T. T. Tjhung, and C. S. Ng. Reply to the comments on: Reduction of peak-to-average power ratio of OFDM system using a companding technique, IEEE Transactions on Broadcasting vol. 45, no.3, September 1999. *IEEE Trans. Broadcast.*, 45(4):420–422, Dec. 1999.

[85] X. Wang, T.T. Tjhung, and C.S. NG. Reduction of peak-to-average power ratio of OFDM system using a companding technique. *IEEE Trans. Broadcast.*, 45(3):303–307, September 1999.

[86] S. G. Wilson. *Digital Modulation and Coding.* Upper Saddle River, NJ: Prentice-Hall, 1996.

[87] B. Wu, S. Cheng, and H. Wang. Clipping effects on channel estimation and signal detection in OFDM. In *IEEE PIMRC*, pages 531 – 534. IEEE, 2003.

[88] Y. Wu and D. A. Pados. An adaptive two-stage algorithm for ML and sub-ML decoding of binary linear block codes. *IEEE Trans. Inform. Theory*, 49(1):261–268, January 2003.

[89] D. Wulich. Comments on the peak factor of sampled and continous signals. *IEEE Commun. Lett.*, 4(7):213–214, July 2000.

[90] X. Li and L. J. Cimini Jr. Effects of clipping and filtering on the performance of OFDM. *IEEE Commun. Lett.*, 2(5):131–133, 1998.

[91] Y. Wu X. Wang, T.T. Tjhung. On the SER and spectral analyses of A-law companded multicarrier modulation. *IEEE Trans. Veh. Technol.*, 52:1408 – 1412, September 2003.

[92] H. Xiao, L. Jianhua, Z. Junli, J. Chuang, and G. Jun. Reduction of peak-to-average power ratio of OFDM signals with companding transform. *IEE Elect. Lett.*, 37(8):506–507, April 2001.

[93] H. Xiao, L. Jianhua, C. Justin, and Z. Junli. Companding transform for the reduction of peak-to-average power ratio of OFDM signals. In *IEEE Vehicular Technology Conference*, pages 835 –839. IEEE, 2001.

[94] Y. Xin and I. J. Fair. High-order spectral- multimode codes. *IEEE Trans. Commun.*, 52(8):1231–1237, August 2004.

[95] Y. Xin and I.J. Fair. A performance metric for codes with a high-order spectral at zero frequency. *IEEE Trans. Inform. Theory*, 50(2):385–394, February 2004.

[96] Y. Xin and Ivan J.Fair. Peak-to-Average Power Ratio Reduction of an OFDM Signal Using Guided Scrambling Coding. In *IEEE GLOBECOM*, pages 2390–2394, 2003.

[97] Kyeongcheol Yang and Seok-Il Chan. Peak-to-average power control in OFDM using standard arrays of linear block codes. *IEEE Commun. Lett.*, 7:174–176, 2003.

[98] Y. You, W. Jeon, J. Paik, and H. Jung. Low-complexity PAR reduction schemes using SLM and PTS approaches for OFDM-CDMA signals. *IEEE Trans. Consumer Electron.*, 49(2):284–289, May 2003.